RESEARCH ARTICLE

Hiding in plain sight: Genomic and phenotypic characterization of mosquito-borne Bussuquara virus

Madeline R. Steck[1], Cecília A. Banho[2], Vsevolod L. Popov[1], Haiping Hao[3], Kathryn A. Hanley[4], Mauricio L. Nogueira[1,2], Nikos Vasilakis[1,5*]

1 Department of Pathology, University of Texas-Medical Branch, Galveston, Texas, United States of America, 2 Laboratório de Pesquisas em Virologia, Faculdade de Medicina de São José do Rio Preto, São José do Rio Preto, São Paulo, Brazil, 3 Department of Biochemistry & Molecular Biology, University of Texas-Medical Branch, Galveston, Texas, United States of America, 4 Department of Biology, New Mexico State University, Las Cruces, New Mexico, United States of America, 5 Center for Vector-Borne and Zoonotic Diseases, University of Texas Medical Branch, Galveston, Texas, United States of America

* nivasila@utmb.edu

Abstract

Bussuquara virus (BSQV), an orthoflavivirus discovered in Brazil in 1956, has been detected throughout the Americas in diverse mosquito and vertebrate species, including humans. Critical gaps in BSQV knowledge include its capacity for urban transmission and clinical pathogenesis outcomes, with insufficient historical experimentation to draw genomic or phenotypic comparisons to related orthoflavivirus species. The objective of this study was to conduct morphologic, genomic, phylogenetic, and *in vitro* viral fitness characterization of BSQV using the four available historical strains. We used next generation sequencing and rapid amplification of cDNA ends to construct consensus genomes, followed by phylogenetic analysis and genome annotation to evaluate orthoflavivirus evolutionary relationships and genome characteristics. Infected mosquito (C6/36) and non-human primate (Vero CCL81) cells were imaged with transmission electron microscopy. Viral replication kinetics were quantified across seventeen cell lines of mosquito, mammal, rodent, avian, non-human primate, and human origin. BSQV morphologic (virion diameter, cytopathic effect) and genomic (size, organization, architecture, sequence motifs) results were in line with canonical orthoflavivirus characteristics. One of the four strains (CoAr 41922) shared greater sequence homology to the Naranjal orthoflavivirus than other BSQV strains and was thus excluded from infection phenotype experiments. All three confirmed BSQV strains replicated robustly in most mosquito and all vertebrate cell lines, causing either minimal (mosquito) or moderate to extreme (vertebrate) cytopathic effects. We conclude that BSQV is a generalist orthoflavivirus with a broad range of susceptible vertebrate and mosquito vectors. Our data build a foundation for pathogenesis

and vector competence studies to determine the potential of BSQV to emerge into epizootic and urban transmission cycles.

Author summary

After decades of being considered negligible pathogens, multiple mosquito-borne viruses, such as Zika and Mayaro, are now recognized as significant human health threats across the neotropics. Bussuquara virus (BSQV) is a mosquito-borne orthoflavivirus discovered in Brazil that is closely related to epidemic orthoflavivirus species; however, the current and potential future threats posed by BSQV to human health are unknown. Our study is the first assessment into BSQV's capacity to become a medically important mosquito-borne virus in the Americas, and we do so by characterizing the BSQV virion morphology, genome, and evolutionary relationships and comparing them to their more well-studied orthoflavivirus relatives. We also investigate the ability of BSQV to infect or impair representative mosquito and vertebrate cells. Our findings demarcate the genomic similarities and differences, implications yet unknown, between BSQV and more prominent orthoflaviviruses. Cell infection studies suggest that BSQV can infect a broad range of mosquito and vertebrate species, with cytopathy uncommon in mosquito cells but prominent in vertebrate cells, including those of human brain, testes, and kidney origins. These data suggest BSQV has the capacity to sustain transmission cycles within human populations by expansion of its vector host range, and to cause human disease.

Introduction

Bussuquara virus (Family: *Flaviviridae*, Genus: *Orthoflavivirus*) was discovered in 1956 in the Amazon rainforest in northern Brazil [1]. BSQV isolations and antibody detection were then reported from multiple mosquito genera (*Culex, Trichoprosopan, Mansonia, Collquilettidia*) and vertebrate taxa (non-human primates, rodents, birds, sloths, bats, ruminants, horses, and humans) [2]. To date, detections are limited to sylvatic and epizootic transmission cycles and there is no reported evidence of urban transmission between domesticated mosquitoes (i.e., *Aedes aegypti* and *Ae. albopictus*) and humans. However, BSQV is known to infect and cause disease in humans, as demonstrated by a self-resolving febrile case in 1970s Panama [3] and detection of convalescent IgG immunity in humans from rainforest-proximate villages in Panama [3] and Argentina [4]. The spectrum of potential clinical manifestations is undefined, although an early animal study [5] demonstrated fatal central nervous system virulence in neonatal hamsters.

The neotropics are hyperendemic for many arthropod-borne viruses (arboviruses); however, only those designated as medically relevant are intentionally surveilled or diagnosed in clinical settings. Multiple mosquito-borne orthoflaviviruses have emerged in the Americas including Zika (ZIKV), dengue (DENV) serotypes 1–4, Ilhéus (ILHV), yellow fever (YFV), Saint Louis encephalitis (SLEV), and Rocio (ROCV) viruses [6–12]. BSQV

is not currently a priority for surveillance, and its detection is further hindered by a lack of commercial diagnostics. Thus, the true infection burden of BSQV in human populations is unknown, since low-level circulation could be masked by inapparent or undifferentiated arboviral symptoms or orthoflavivirus cross-reactivity in serological assays [13].

It is critical to proactively assess the emergence risk of neglected arboviruses. Recent decades illustrate the challenges of mitigating unforeseen arbovirus emergence events including accurate diagnosis, interrupting transmission, or providing effective therapeutics [14–16]. With five hundred arbovirus species listed in the US Centers for Disease Control Arbovirus Catalog (ArboCat) [17], comprehensive characterization of each virus is not feasible. A rational approach is to prioritize arbovirus species with potential to (i) sustain urban transmission and (ii) threaten human health. The historical literature implicates BSQV as a generalist *Culex*-vectored orthoflavivirus with a broad range of susceptible vertebrate species, including humans [2]. Here we sought to evaluate this interpretation of early BSQV studies by analyzing its genome, infection phenotype, evolutionary relationships, and infection kinetics using all available BSQV isolates.

Materials and methods

Cells and viruses

A panel of mosquito (n = 7) and vertebrate (n = 10) cell lines were used to assess BSQV replication kinetics (Table 1). Vertebrate and mosquito cells were maintained using the maintenance media described below in a humidified incubator with 5% CO_2, at 37°C or 28°C, respectively, excluding CxTr and CT cells which were maintained at 28°C without CO_2 or humidity. Infection media used 2% FBS, except HSerC cell infection media which retained 10% FBS. CxTr was obtained from the Foreign Arthropod-Borne Animal Disease Research Unit (US Department of Agriculture, Manhattan, KS, USA), while Hsu and CT were both gifted by the Ebel lab at Colorado State University, Fort Collins, CO. HserC cells were purchased from iXCells Biotechnologies (San Diego, California, USA). All other cell lines originated from the American Type Culture Collection (ATCC, Manassas, VA, USA).

Three BSQV strains (BeAn 217201, BeAn 4116, CoAr 41922) were obtained from the World Reference Center for Emerging Viruses and Arboviruses (University of Texas Medical Branch, Galveston, TX, USA). The prototype BSQV strain, BeAn 4073, was sourced from ATCC. Passage history of the lyophilized stocks upon receipt is noted in Table 2. Vero CCL81 cells were infected with each strain for one passage until >50% ablation of the monolayer (2–3 days). Infected cell culture supernatant was collected, clarified through centrifugation, supplemented with 1X SPG buffer, and stored at -80°C until experimental use. Two strains (BeAn 4116, BeAn 217201) had one extra passage in Vero CCL81 cells supplemented with 25µg/ml Plasmocin antibiotic (InvivoGen, San Diego, CA, USA) before stock expansion.

Virus quantification

Vero CCL81 cells were seeded onto 24-well plates to reach ~80% confluency by the following day (~24 hours). Monolayers were then infected with 100µL/well of inoculum, with triplicate wells of sample dilutions (10^{00}-10^5) in infection media (**Table 1**) per virus strain and day. Plates were incubated at 37°C with 5% CO_2 for one hour with rocking every fifteen minutes. A methylcellulose overlay - 0.8% methyl cellulose (Sigma-Aldrich), 1X MEM, 3% FBS, 1% P/S - was added to cells for 3 (BeAn 217201) or 4 (BeAn 4116, BeAn 4073) day incubation. The methylcellulose overlay was then removed, and monolayers were fixed with 1:1 acetone:methanol solution at room temperature for one hour, followed by washing and drying. All wells were stained with 0.2% (vol/vol) crystal violet (Sigma-Aldrich) in methanol (Sigma-Aldrich). Plaques were counted, averaged between the three replicates, and quantified as plaque forming units per milliliter supernatant (PFU/mL).

Viral RNA extraction

Viral RNA was extracted and purified following a standard protocol [19] using Trizol reagent (InvivoGen) and chloroform (Sigma-Aldrich). The final RNA pellet was resuspended (~2ng/µL) in 20µL of RNase/DNase and protease-free water (Ambion, Austin, TX, USA) and frozen at -80°C until sequencing or RACE analyses.

Table 1. Cell lines and culture media compositions.

Cell Line	Species	Common Name	Tissue	Base Media	Supplements
Vero CCL81	*Cercopithecus aethiops*	African green monkey	kidney epithelium	DMEM	10% FBS, 1% P/S
FRhL-2	*Macaca mulatta*	Rhesus macaque	lung fibroblasts	EMM	10% FBS, 1% P/S
BHK-21	*Mesocricetus auratus*	Golden Syrian hamster	kidney fibroblasts	DMEM	10% FBS, 1% P/S
OK	*Didelphis marsupialis virginiana*	North American opposum	kidney epithelium	MEM	10% FBS, 1% P/S
Huh7	*Homo sapiens*	Human	hepatoma	DMEM	10% FBS, 1% P/S, 1% NaPy, 1% NEAA
SH-SY5Y	*Homo sapiens*	Human	neuroblastoma	DMEM	10% FBS, 1% P/S
HSerC	*Homo sapiens*	Human	human testis	SCBGM	10% FBS, 1% AA
A549	*Homo sapiens*	Human	lung epithelium	DMEM	10% FBS, 1% P/S
QM7	*Coturnix coturnix japonica*	Japanese quail	muscle	M199	10% FBS, 1% P/S, 10% TPB
LMH	*Gallus gallus*	Chicken	liver epithelium	WMB	10% FBS, 1% P/S*
C6/36	*Ae. albopictus*	Mosquito	larvae	DMEM	10% FBS, 10% TPB,1% P/S, 1% AmpB
C7-10	*Ae. albopictus*	Asian tiger mosquito	larvae	DMEM	10% FBS, 1% P/S, 1% NaPy, 1% NEAA
U4.4	*Ae. albopictus*	Asian tiger mosquito	larvae	M&M	20% FBS, 5% TPB, 1% P/S, 0.15% NaHCO$_3$.
Aag2	*Ae. aegypti*	Yellow fever mosquito	larvae	DMEM	20% FBS, 2% NaHCO$_3$, 1% TPB, 1% P/S, 1% NEAA
Hsu	*Cx. quinque-fasciatus*	Southern house mosquito	ovaries	DMEM	10% FBS, 10% TPB,1% P/S, 1% AmpB
CT	*Cx. tarsalis*	Western encephalitis mosquito	embryonated eggs	SDM	10% FBS, 1% P/S,1% AmpB
CxTr	*Cx. tarsalis*	Western encephalitis mosquito	embryonated eggs	SDM	As described in [18]

Species and tissue origins are noted for each cell line, alongside base media and supplements composing maintenance media. Abbreviations: DMEM = Dulbecco's Modified Eagle's Medium (ThermoFisher Scientific, Grand Island, NY, USA); EMEM = Eagles Minimal Essential Medium with L-glutamine (ATCC); MEM = Minimum Essential Media (ThermoFisher Scientific); SCBGM = Sertoli Cell Basal Growth Medium (iXCells Biotechnologies); SDM = Schneider's Drosophila Media (ThermoFisher Scientific); M&M = Mitsuhashi and Maramorosch Insect Medium (HIMEDIA, Kelton, PA, USA); M199 = Medium 199 with Earl's BSS (ThermoFisher Scientific); WMB = Waymouth's MB 752/1 (ThermoFisher Scientific); FBS = heat inactivated fetal bovine serum (ThermoFisher Scientific); P/S = Penicillin–streptomycin (100 U/mL and 100 µg/mL, respectively)(ThermoFisher Scientific); NaPy = 100mM sodium pyruvate (ThermoFisher Scientific); NEAA = 100x non-essential amino acids)(Sigma-Aldrich, Burlington, MA, USA); TBP = Tryptose phosphate broth (ThermoFisher Scientific); AmpB = 250µg/mL Amphotericin B (ThermoFisher Scientific); NaHCO$_3$ = 7.5% w/v sodium bicarbonate (Corning, Corning, NY, USA); AA = Antibiotic-Antimyocitic (iXCells Biotechnologies).

https://doi.org/10.1371/journal.pntd.0013774.t001

Table 2. BSQV strains.

Virus strain	Year	Location	Species	Common Name	Passage History
BeAn 217201	1972	Brazil	*Proechimys guyannensis*	Guyenne spiny rat	SM-1, Vero-2
BeAn 4116	1956	Brazil	*Alouatta belzebul*	Red-handed howler	SM-1, Vero-2
BeAn 4073	1956	Brazil	*Alouatta belzebul*	Red-handed howler	SM-7
CoAr 41922	1960	Colombia	*Culex spp.*	Common House Mosquito	SM-1, Vero-2

Isolation year, country, and species origin recorded for each BSQV strain, and passage history upon receipt. Virus stock preparation required one (BeAn 4073) or two (BeAn 217201, BeAn 4116) additional Vero CCL81 passages before experimental use.

https://doi.org/10.1371/journal.pntd.0013774.t002

Next generation sequencing

Viral RNA (~0.9μg) was fragmented by incubation at 94°C for 15 minutes in 11.5μL of First Strand Reaction Buffer and Random Primer Mix (New England Biolabs, Ipswich, MA). A sequencing library was prepared from the sample RNA using NEBNext Ultra II RNA Library Preparation Kit for Illumina (New England Biolabs) following the manufacturer's protocol. Samples were sequenced on a MiniSeq (Illumina, San Diego, CA) in paired-end 75 base format. Reads in fastq format were quality-filtered, and any adapter sequences were removed, using Trimmomatic software [20]. The virus genomes were assembled using ABySS version 2.3.4 with a range of different kmer sizes and different number of reads. The assembled contigs were then clustered using CD-HIT version 4.8.1 [21] and the resulting contig sequences were blasted against a custom database (entirety of viral protein sequences in GenBank UniProt database) using blastp and against nr nucleotide data base using blastn of NCBI Blast version 2.11.0. The blast hits were then manually curated to assemble into complete genome. The full set of trimmed reads were then aligned to the assembled genome using BWA version 0.7.17 to provide accurate alignment for variants calling with lofreq version 2.1.3.1 [22]. The full sets of raw reads were also aligned to the assembled genome using bowtie2 version 2.3.4.1 [23] to enable quantification of percent viral sequences across the reads. A total of 11.04, 8.06, 15.82, and 7.82 million read pairs were generated for the samples containing BSQV strains BeAn 217201, BeAn 4116, BeAn 4073, and CoAr 41922, respectively. Read pairs mapping to the virus in each sample comprised ~1.8 million (BeAn 217201, 16.7%), ~1.7 million (BeAn 4116, 21.29%), ~1.1 million (BeAn 4073, 7.0%), and ~890,000 (CoAr 41922, 11.38%), respectively.

Rapid amplification of cDNA ends (RACE)

The genomic termini of three BSQV strains BeAn 217201, BeAn 4116, and BeAn 4073 were determined using the kits 5' RACE System for Rapid Amplification of cDNA Ends and 3' RACE System for Rapid Amplification of cDNA Ends (Invitrogen, Vilnius, Lithuania) following manual instructions. Viral RNA from each strain was extracted with the Trizol-chloroform method as outlined above. Consensus BSQV primers were generated using DNASTAR LaserGene primer design tool with default parameters. The *E. coli* RNA Poly(A) Polymerase Kit (New England Biolabs) was used to add a polyadenylated tail to the viral RNA prior to cDNA synthesis for 3' RACE. The 3' termini were PCR amplified first using the primer BSQV_3out (5'- GCCACTGCACTGTACTTCCT-3'), followed by a secondary nested PCR amplification with the primer BSQV_3in (5'-TGATCCCAGGCGAAGGACTA-3') in the forward orientation. The thermocycler (Applied Biosystems, California, USA) conditions for both amplification steps are as follows: 94°C for 3min; 94°C for 1min, 55°C for 1min, 72°C for 70sec (35 cycles); 72°C for 10min. The primer BSQV_5out (5'-TCCAACGTCCATTGCCATGA-3') in the reverse orientation was used for first strand synthesis of the 5' termini, followed by cDNA purification using the QIAquick PCR Purification Kit (Qiagen, Maryland, USA), in lieu of purification with the recommended S.N.A.P. columns. The primer BSQV_5in (5'-TGATCCCAGGCGAAGGACTA-3') in the reverse orientation was used for PCR amplification using the following thermocycler conditions: 94°C for 3min; 94°C for 1min, 62°C for 1min, 72°C for 70sec (35 cycles); 72°C for 10min. The approximately 1090, 250, and 320 nucleotide fragments from amplification with BSQV_3out, BSQV_3in, and BSQV5_in primers, respectively, were separated by 1% agarose gel electrophoresis and purified with the QIAquick Gel Extraction Kit (Qiagen). For Sanger sequencing, PCR products were labeled using BrilliantDye version 3.1 reaction premix (NimaGen, Nijmegen, Netherlands). Labeled products were resolved and read on a SeqStudio 24 Flex Genetic Analyzer (Applied Biosystems) using a 50 cm capillary array and Pop 7 polymer. Results were analyzed using Sequencing Analysis version 8 from Applied Biosystems.

Genome annotation

A sequence alignment of BeAn 217201, BeAn 4073, and BeAn 4116 was compared against protein annotations in NCBI GenBank accession NC_009026.2 to designate 3' and 5' untranslated regions (UTR) and the open reading frame (ORF) including three structural and seven nonstructural proteins. The NetPhos 3.1 server was used to predict post-translational

phosphorylation of residues (serine, threonine, tyrosine), with scores above 0.8 reported here. The NetNglyc server was used to predict post-translational glycosylation of asparagines; positive N-Glyc agreement results (potential >0.5) are reported here, considered high confidence for predictions with 8/9 or 9/9 jury agreement. Viral (NS2B/NS3) and host proteases (furin, signalase, unknown) cleavage enzymes were designated based on previous reviews of proteases associated with orthoflavivirus replication [24–30]. Cysteine bridges and transmembrane domains were predicted based on alignments with other orthoflaviviruses [31–40]. Secondary RNA structures at the flanking 5' and 3' UTR were predicted using the RNA folding form on the UNAFold webserver [41]. Folding parameters included selection of external loop (flat_alt) algorithm [natural (5'UTR), untangle (3'UTR)], and maximum base pair distance of 80 nucleotides for the 3' UTR. Complementary sequence motifs in the 5' and 3' UTR including upstream AUG region (UAR), downstream AUG region (DAR), and cyclization sequence (CS) were predicted based on alignments with published orthoflavivirus sequence elements [42–50].

Nucleotide sequence accession numbers

The four consensus sequences were uploaded onto NCBI GenBank under the following accession numbers: PV035816 (BeAn 217201), PV035817 (BeAn 4116), PV035818 (BeAn 4073), and PV035818 (CoAr 41922).

Phylogenetic analysis

The phylogenetic analysis was performed using a curated dataset of eighty-one genomes (prototype strains prioritized)[51–56] retrieved from NCBI GenBank, of mosquito-borne (MB), tick-borne (TB), no known vector (NKV), and a subset of insect specific (IS) orthoflavivirus species, alongside the four novel consensus sequences (S1 Table). MacVector version 18.5.1 was used to isolate the ORF nucleotide sequence, followed by codon translation and amino acid alignment using MAFFT multiple sequence alignment software version 7.271 [57], according to the accuracy-oriented method E-INS-i. Next, a maximum-likelihood (ML) phylogenetic tree was reconstructed in IQ-TREE v. 2.2.2.6 [58] using the best-fit model of amino acid substitution according to the Bayesian information criterion (BIC) inferred by the ModelFinder tool [59]. The reliability of branching patterns was tested using a combination of ultrafast bootstrap (UFBoot) and the SH-like approximate likelihood-ratio test (SH-aLRT) [60,61] with percent support values of 95% and 80%, respectively, considered thresholds of high confidence in nodal support. The final tree was visualized and edited in FigTree 1.4.4.

Transmission electron microscopy

Individual T-25 flasks were seeded with Vero CCL81 or C6/36 cells and then infected next day with one of three BSQV strains; BeAn 217201, BeAn 4116, or BeAn 4073. Upon observation of cytopathic effect (CPE)(e.g., plaque formation) in Vero CCL81 monolayers (~24 hours), supernatant was removed from both Vero CCL81 and C6/36 cultures, then monolayers immediately fixed and stored at 4 °C for at least 24 hours. Fixation reagent was a mixture of 2.5% formaldehyde prepared from paraformaldehyde powder, and 0.1% glutaraldehyde in 0.05M cacodylate buffer pH 7.3 to which 0.01% picric acid and 0.03% $CaCl_2$ were added. For ultrastructural analysis in ultrathin sections, the monolayers were washed in 0.1 M cacodylate buffer, cells were scraped off and processed further as a pellet. The pellets were post-fixed in 1% OsO_4 in 0.1M cacodylate buffer pH 7.3 for 1 hr, washed with distilled water and *en bloc* stained with 2% aqueous uranyl acetate for 20 min at 60°C. The pellets were dehydrated in ethanol, processed through propylene oxide and embedded in Poly/Bed 812 (Polysciences, Warrington, PA). Ultrathin sections were cut on Leica EM UC7 ultramicrotome (Leica Microsystems, Buffalo Grove, IL), stained with lead citrate and examined in a JEM-1400 (JEOL USA, Peabody, MA) transmission electron microscope at 80 kV. Digital images were acquired with a bottom-mounted CCD camera Orius SC200 1 (Gatan, Pleasanton, CA).

Replication kinetics

Cells were seeded onto 12-well plates with maintenance media (Table 1) to reach ~80% confluency in 1–2 days. BSQV strains (BeAn 217201, BeAn 4116, BeAn 4073) at MOI = 0.01 were used to inoculate cell monolayers by one hour incubation with tilting of plates every 15 min, in the respective 28°C (mosquito cells) or 37°C (vertebrate cells) incubator. Wells were washed three times with PBS and overlaid with 2mL infection media, with 250µL immediately removed and titrated to assess measure carryover virus (e.g., 0 dpi). The entirety of media was collected and replaced with fresh infection media every 24 hours up to 12 dpi. Collected media was clarified by low-speed centrifugation and titrated on Vero CCL81 cells the same day following the described virus quantification protocol. Comparisons of monolayer integrity between BSQV strains were recorded every other day using a CKX53 inverted microscope (Olympus, Waltham, MA) with the 10×CACHN-IPC objective lens (Olympus) and an attached EP50 digital camera (Olympus).

Statistical analysis

JMP Pro 18 software (JMP Statistical Discovery, Cary, NC, USA) was used for all statistical tests and graphs. Viral titers (PFU/mL) were $\log_{10}$-transformed to assess the overall and daily BSQV strain variation during replication kinetics experiments using two-way repeated measures ANOVA and Tukey's multiple comparisons test. Values below the limit of detection (< 1 plaque produced in Vero monolayer with infection of 100µL undiluted sample) were treated as 0.9 $\log_{10}$ PFU/mL for graphing and statistical purposes. Effects of BSQV strain, day, and the interaction between strain and day were tested.

Results and discussion

Genome characterization

NCBI BLAST results confirmed BeAn 217201 and BeAn 4116 strains as BSQV, and ClustalW multiple sequence alignment demonstrated high congruency of both isolates to the archived (NCBI: NC_009026) and novel (PV035818) sequences of the prototype strain, BeAn 4073 (Table 3). The NCBI reference genome differs by seven additional nucleotides in the 3'UTR with the offset appearing between sites 11514–11579. Our four novel consensus sequences have a matched ORF length (3430aa); however, the CoAr 41922 strain has a longer 5'UTR (125nt) and 3'UTR (704nt) compared to the 5'UTR (104nt) and 3'UTR (438nt) of BeAn 217201, BeAn 4116, and BeAn 4073. The CoAr41922 strain shares higher nucleotide (80.93%) and amino acid (95.69%) homology with Naranjal virus (NAJV) (NCBI: KF917538), another member of the *Aroa* virus group (*Orthoflavivirus aroaense*), compared to the other three BSQV strains. The International Committee on Taxonomy of Viruses lists orthoflavivirus species demarcation criteria as (i) nucleotide and deduced amino acid sequence data, (ii) antigenic characteristics, (iii) geographic association, (iv) vector association, (v) host association, (vi) disease association, and (vii) ecological characteristics [62]. With limited ecological knowledge of Aroa serocomplex species, we concluded that CoAr41922 was not BSQV based on genetic homology, and this strain was thereby excluded from further genomic annotation or replication kinetics studies.

Phylogeny

Each of the four consensus sequences are clustered within the Aroa serocomplex (Fig 1). The BeAn 217201 strain diverged prior to the shared node between BeAn 4073 and BeAn 4116, which displayed the closest evolutionary history. Notably, these two strains were isolated from sequential blood draws, three days apart, from a sentinel non-human primate (*Alouatta belzebul,* red howler monkey) near Belem, Para State, Brazil [1] (Table 1). Meanwhile, BeAn 217201 was isolated from a sylvatic rodent (*Proechimys* sp.*,* spiny rat) within the same region. The CoAr 41922 strain shares a node with NAJV with clear divergence from the BSQV isolates. There are no additional NAJV genomes available, thus the evolutionary history between the NAJV prototype (isolated 1976, Ecuador, sentinel hamster) [27] and CoAr 41922, lacks clarity.

Table 3. ORF sequence comparisons across Aroa serocomplex.

Nucleotide	BeAn 4073	BeAn 4116	BeAn 217201	CoAr 41992	KF917538	KF917535	AY632538
BeAn 4073	100.0	99.9	97.3	75.8	75.0	61.6	61.6
BeAn 4116	99.9	100.0	97.3	75.8	75.0	61.7	61.7
BeAn 217201	97.3	97.3	100.0	76.1	75.1	61.7	61.6
CoAr 41992	75.8	75.8	76.1	100.0	80.9	61.3	61.2
KF917538	75.0	75.0	75.1	80.9	100.0	61.8	61.3
KF917535	61.6	61.7	61.7	61.3	61.8	100.0	76.7
AY632538	61.6	61.7	61.6	61.2	61.3	76.7	100.0
Amino Acid	**BeAn 4073**	**BeAn 4116**	**BeAn 217201**	**CoAr 41992**	**KF917538**	**KF917535**	**AY632538**
BeAn 4073	100.0	99.9	99.4	86.9	86.8	77.5	60.8
BeAn 4116	99.9	100.0	99.4	86.9	86.8	77.5	60.7
BeAn 217201	99.8	99.8	100.0	87.0	86.8	77.5	60.8
CoAr 41992	94.9	94.9	95.0	100.0	95.7	77.3	60.6
KF917538	94.8	94.9	94.9	98.7	100.0	77.4	76.7
KF917535	61.2	61.2	61.3	61.1	61.2	100.0	88.5
AY632538	77.0	77.0	77.0	76.6	60.9	96.0	100.0

ClustalW multiple sequence alignments were performed with MacVector version 18.5.1 to produce square matrices quantifying both percent sequence identity and sequence similarity of BeAn 217201, BeAn 4116, BeAn 4073, and CoAr 41922 against nucleotide (**top**) or (**bottom**) amino acid ORF sequences against Aroa serocomplex species. Prototype sequences (accession, isolate) retrieved from NCBI GenBank for AROAV (KF917535, Macaray 01809), NAJV (KF917538, 25008), and IGUV (AY632538, SPAn 71686). Similarity scores (%) are shown below the diagonal with identity scores (%) above.

https://doi.org/10.1371/journal.pntd.0013774.t003

Transmission electron microscopy

In ultrathin sections of Vero and C6/36 cells, approximately 19 hours post-infection, all examined virus strains displayed similar morphology of intracytoplasmic membranes transformation characteristic of orthoflaviviruses: formation of convoluted membranes (CM) and smooth membrane structures (SMS) within the cisterns of granular endoplasmic reticulum (ER) which represent orthoflavivirus replication complexes (Fig 2A-2C, 2E, and 2F). Within the expanded cisterns of granular ER, immature virions ~40 nm in diameter could be observed (Fig 2C-2E, arrows).

Genome annotation

5' and 3'UTRs. Two strains, BeAn 4073 and BeAn 4116, were 100% identical at the nucleotide level within the 5' and 3' UTR, with six divergent nucleotides compared to BeAn 217201. The characteristic stem-loops, dumbbells, and hairpin structures associated with the folded orthoflavivirus genome [63,64] were visualized for all three strains, with one structure representing both BeAn 4116 and BeAn 4073 (Figs 3 and 4). The BSQV 5' UTR spans nucleotides 1–104; however, for structure prediction software, an additional forty-eight nucleotides following the first AUG codon (up to the second AUG codon) were included. This allowed incorporation of the orthoflavivirus capsid hairpin (CHP) (Fig 3) which is instrumental in first AUG codon selection during viral translation [64]. The previous BSQV 5'UTR structure prediction [65] neglected to include these additional capsid coding nucleotides. There was a single nucleotide change between strains at position 23 that did not impact predicted final structure. The BSQV 5' UTR also includes two conserved stem loop structures; SLA is associated with promoting the viral RNA polymerase and genome capping, while SLB contains the first AUG and the 5' UAR [63,64].

Long-range RNA:RNA interactions, via pairing of short complementary regions (UAR, DAR, CS) between the 5' UTR and 3'UTR, are critical for orthoflavivirus genome circularization and subsequently, orthoflavivirus replication and translation [63,66–68]. The BSQV genome contains these cyclization motifs (S2 Table) in the approximate sites and with similar
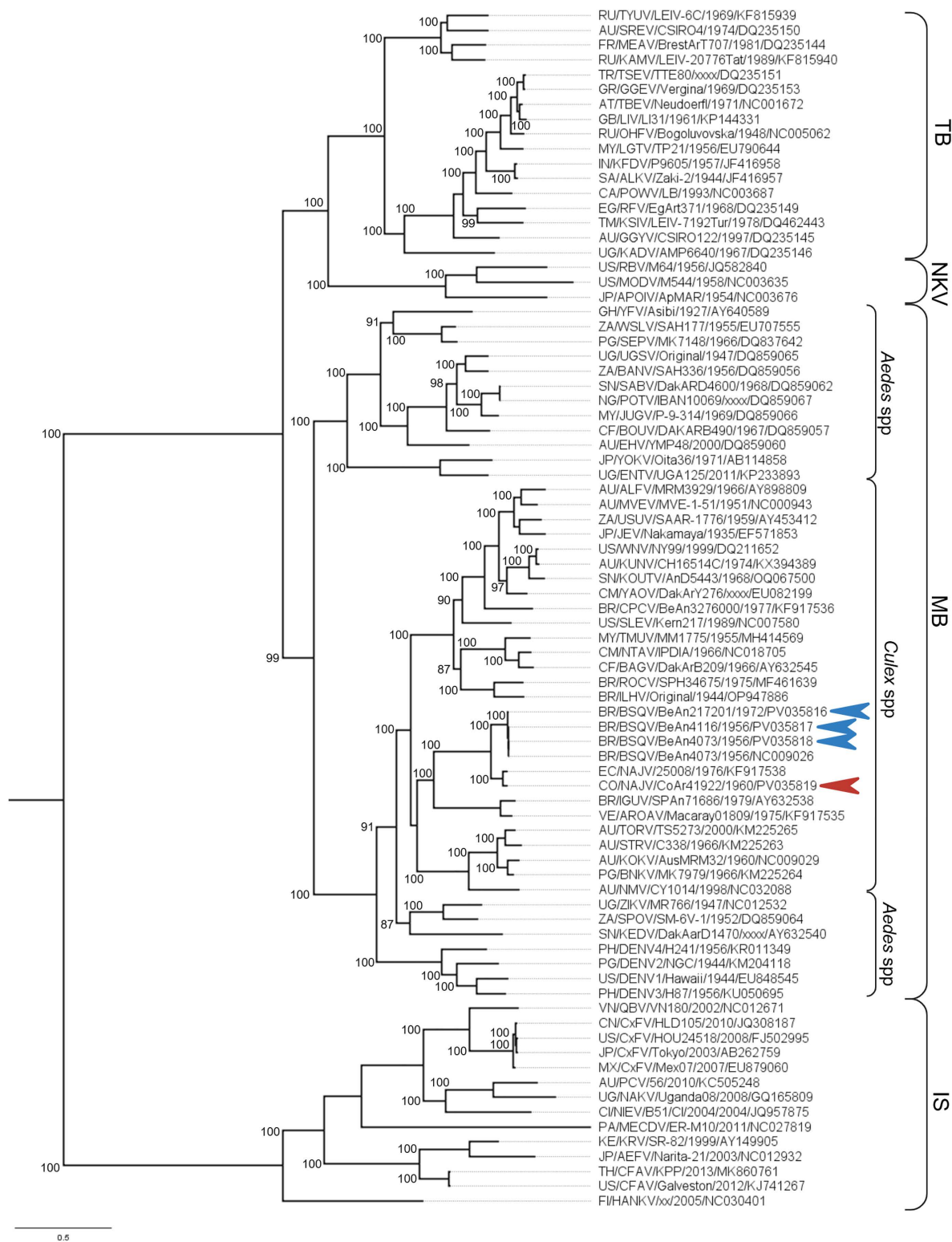
RU/TYUV/LEIV-6C/1969/KF815939
AU/SREV/CSIRO4/1974/DQ235150
FR/MEAV/BrestArT707/1981/DQ235144
RU/KAMV/LEIV-20776Tat/1989/KF815940
TR/TSEV/TTE80/xxxx/DQ235151
GR/GGEV/Vergina/1969/DQ235153
AT/TBEV/Neudoerfl/1971/NC001672
GB/LIV/LI31/1961/KP144331
RU/OHFV/Bogoluvovska/1948/NC005062
MY/LGTV/TP21/1956/EU790644
IN/KFDV/P9605/1957/JF416958
SA/ALKV/Zaki-2/1944/JF416957
CA/POWV/LB/1993/NC003687
EG/RFV/EgArt371/1968/DQ235149
TM/KSIV/LEIV-7192Tur/1978/DQ462443
AU/GGYV/CSIRO122/1997/DQ235145
UG/KADV/AMP6640/1967/DQ235146
US/RBV/M64/1956/JQ582840
US/MODV/M544/1958/NC003635
JP/APOIV/ApMAR/1954/NC003676
GH/YFV/Asibi/1927/AY640589
ZA/WSLV/SAH177/1955/EU707555
PG/SEPV/MK7148/1966/DQ837642
UG/UGSV/Original/1947/DQ859065
ZA/BANV/SAH336/1956/DQ859056
SN/SABV/DakARD4600/1968/DQ859062
NG/POTV/IBAN10069/xxxx/DQ859067
MY/JUGV/P-9-314/1969/DQ859066
CF/BOUV/DAKARB490/1967/DQ859057
AU/EHV/YMP48/2000/DQ859060
JP/YOKV/Oita36/1971/AB114858
UG/ENTV/UGA125/2011/KP233893
AU/ALFV/MRM3929/1966/AY898809
AU/MVEV/MVE-1-51/1951/NC000943
ZA/USUV/SAAR-1776/1959/AY453412
JP/JEV/Nakamaya/1935/EF571853
US/WNV/NY99/1999/DQ211652
AU/KUNV/CH16514C/1974/KX394389
SN/KOUTV/AnD5443/1968/OQ067500
CM/YAOV/DakArY276/xxxx/EU082199
BR/CPCV/BeAn3276000/1977/KF917536
US/SLEV/Kern217/1989/NC007580
MY/TMUV/MM1775/1955/MH414569
CM/NTAV/IPDIA/1966/NC018705
CF/BAGV/DakArB209/1966/AY632545
BR/ROCV/SPH34675/1975/MF461639
BR/ILHV/Original/1944/OP947886
BR/BSQV/BeAn217201/1972/PV035816
BR/BSQV/BeAn4116/1956/PV035817
BR/BSQV/BeAn4073/1956/PV035818
BR/BSQV/BeAn4073/1956/NC009026
EC/NAJV/25008/1976/KF917538
CO/NAJV/CoAr41922/1960/PV035819
BR/IGUV/SPAn71686/1979/AY632538
VE/AROAV/Macaray01809/1975/KF917535
AU/TORV/TS5273/2000/KM225265
AU/STRV/C338/1966/KM225263
AU/KOKV/AusMRM32/1960/NC009029
PG/BNKV/MK7979/1966/KM225264
AU/NMV/CY1014/1998/NC032088
UG/ZIKV/MR766/1947/NC012532
ZA/SPOV/SM-6V-1/1952/DQ859064
SN/KEDV/DakAarD1470/xxxx/AY632540
PH/DENV4/H241/1956/KR011349
PG/DENV2/NGC/1944/KM204118
US/DENV1/Hawaii/1944/EU848545
PH/DENV3/H87/1956/KU050695
VN/QBV/VN180/2002/NC012671
CN/CxFV/HLD105/2010/JQ308187
US/CxFV/HOU24518/2008/FJ502995
JP/CxFV/Tokyo/2003/AB262759
MX/CxFV/Mex07/2007/EU879060
AU/PCV/56/2010/KC505248
UG/NAKV/Uganda08/2008/GQ165809
CI/NIEV/B51/CI/2004/2004/JQ957875
PA/MECDV/ER-M10/2011/NC027819
KE/KRV/SR-82/1999/AY149905
JP/AEFV/Narita-21/2003/NC012932
TH/CFAV/KPP/2013/MK860761
US/CFAV/Galveston/2012/KJ741267
FI/HANKV/xx/2005/NC030401

TB
NKV
Aedes spp
MB
Culex spp
Aedes spp
IS

0.5

Fig 1. Phylogenetic relationship of BSQV strains. Maximum-likelihood tree for the *Orthoflavivirus* genus based on complete amino acid sequences of eighty-one species across four vector-associated clades (right-most brackets); TB, MB, NK, and IS orthoflaviviruses. Numbers in parentheses at major branch nodes are UFBoot (%); only thresholds over 80% are shown. The scale bar depicts a genetic distance of 0.5 or 50% nucleotide sequence

divergence by site. MB subclades of principal vector genera (*Aedes, Culex*) are indicated by innermost brackets. Consensus sequences of confirmed BSQV (n = 3)(blue arrow) and NAJV (n = 1)(red arrow) isolates. Node labels depict country code/ virus name/ isolate/ year/ NCBI accession. Subclades are listed as: mosquito-borne (MB), tick-borne (TB), insect specific (IS), or no known vector (NKV). The final tree was visualized and edited in FigTree v1.4.4, with supplementary brackets, arrows, and labels (node values, vector clade) added at Biorender.com (https://BioRender.com/5ov1u7j).

sequence lengths (UAR: 12–18 nt, DAR: 3–6 nt per domain, CS:10–18 nt) as other orthoflaviviruses [42,50]. Orthoflaviviruses are shown to have one to two DAR [42,69]; BSQV has one DAR domain and the CS and UAR sequence lengths at the range minima.

   The BSQV 3' UTR spans nucleotides 10395–10808. Unlike the BSQV 5' UTR, there was variation in predicted RNA folding between strains, as seen with the incongruent stem loop preceding the sHP and terminal 3' SL (Fig 4) due to variation nucleotide positions 10693 and 10694. An orthoflavivirus 3'UTR is composed of three domains (I-III). Domain I is the most variable in architecture and contains tandem SLs that function as exoribonuclease XRN1 resistant RNA (xrRNA) structures [67]. All BSQV strains have one predicted stem loop followed by a shorter hairpin in this domain, indicating one xrRNA (Fig 4) matching previous genus-wide analyses [70,71]. BeAn217201 differs from the other two strains by one nucleotide (10490) in Domain I in the small hairpin (Fig 3).
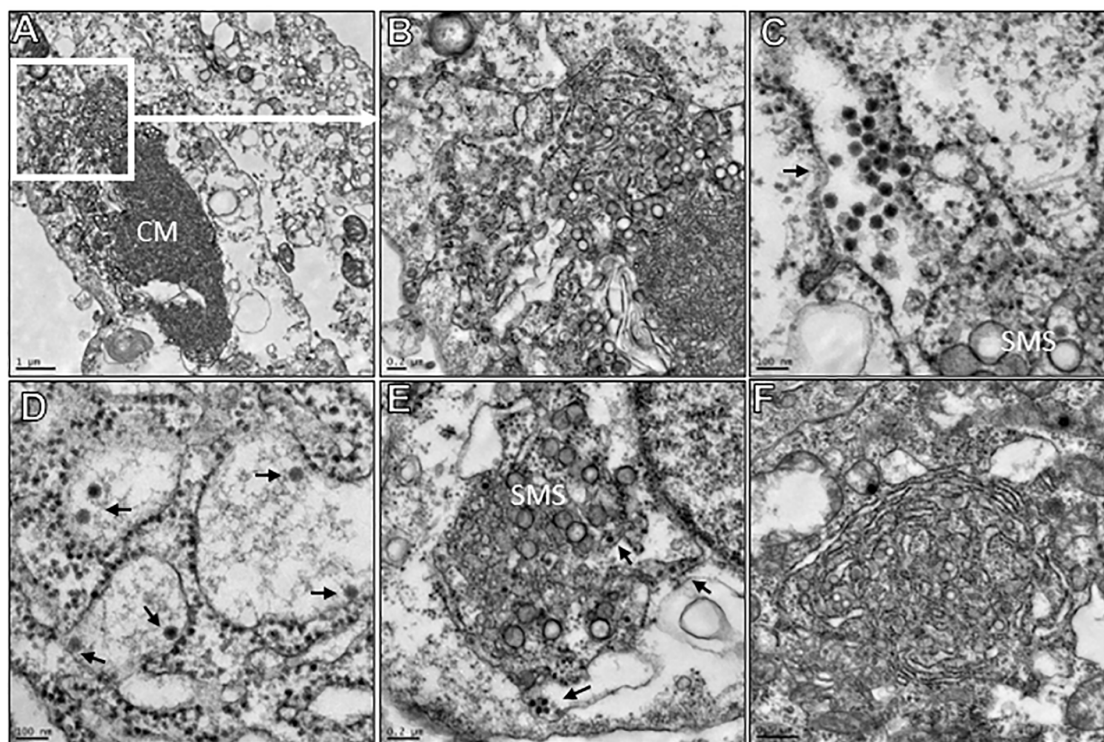

Fig 2. Ultrastructure of BSQV viruses in ultrathin sections. (A) BeAn 217201 in Vero cells. Replication complex presented by convoluted membranes (CM) and smooth membrane structures (SMS). Bar = 1 um. **(B)** Fragment of Fig 1A demonstrates immature virions and SMS within the lumen of granular ER. Bar = 0.2 um. **(C)** BeAn 4116 in a Vero cell. Cluster of immature virions (arrow) in a lumen of expanded granular ER. Bar = 100 nm. **(D)** BeAn 4116 in a C6/36 cell. Individual immature virions (arrows) within an expanded cistern of granular ER. Bar = 100 nm. **(E)** BeAn 4073 in a Vero cell. SMS and single immature virions (arrows) within a conglomerate of granular ER cisterns. Bar = 0.2 um. **(F)** BeAn 4073 in a C6/36 cell. SMS within a tight conglomerate of granular ER cisterns. Bar = 0.5 um.
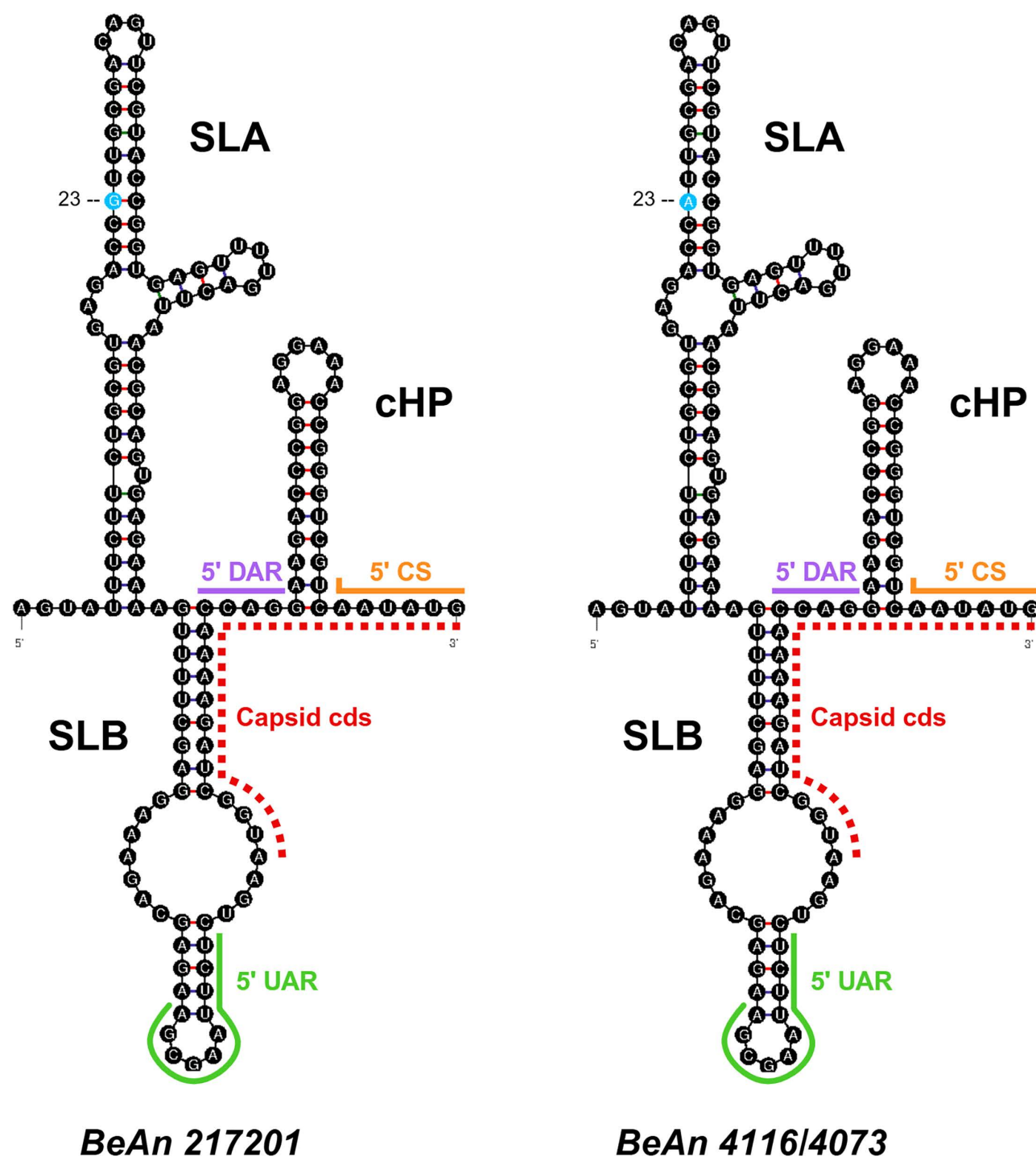
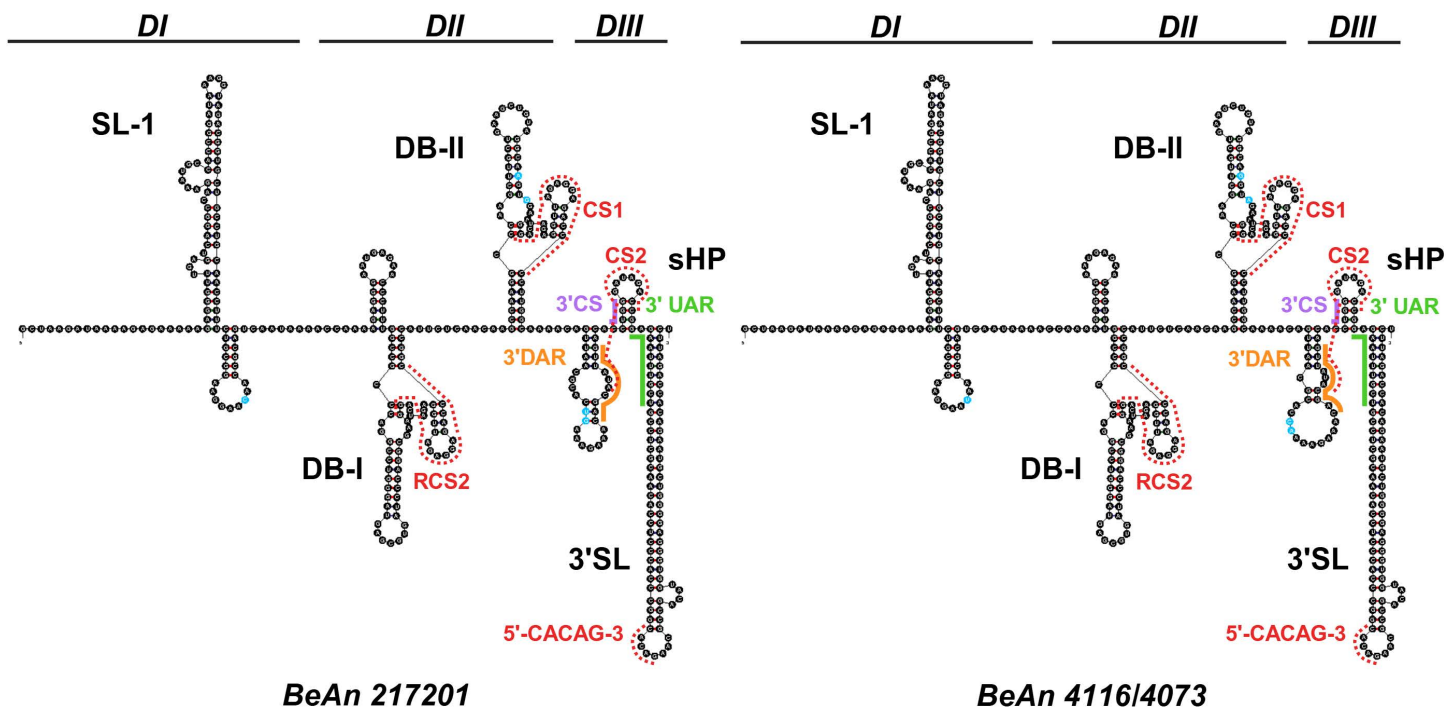**Fig 3. Predicted 5' UTR secondary structure.** Canonical orthoflavivirus RNA structural elements present in predicted folding of BSQV strains. Conformations include two stem loops (SLA, SLB) and the capsid hairpin (cHP) within the 5' UTR. The capsid protein coding sequence (cds) from the first to second start codon (AUG) was included for software prediction. Nucleotide differences between strains are highlighted in blue. The complementary UAR, DAR, and CS (partial) are color coded to indicate pairing with 3' UTR motifs in Fig 4. The loop free-energy decomposition (ΔG) values for structure predictions are 49.20 (BeAn 217201) and 45.80 (BeAn 4116/4073). Structure prediction originates from UNAFold Web Server and supplementary graphics added at Biorender.com (https://BioRender.com/qtzxxxr).

https://doi.org/10.1371/journal.pntd.0013774.g003

Fig 4. Predicted 3' UTR secondary structure. Canonical orthoflavivirus RNA structural elements present in predicted folding include: two stem loops (SL-I, 3'SL), two dumbbells (DB-I, DB-II), and the short hairpin (sHP) across the three domains (DI-III). Nucleotide differences between strains are highlighted in blue. The complementary UAR, DAR, and CS are color coded to indicate pairing with 5' UTR motifs in Fig 3. The conserved 5'CACAG'3' pentanucleotide and RCS/CS sequences are outlined with red dashes. The loop free-energy decomposition (ΔG) values for structure predictions are 136.36 (BeAn 217201) and 132.10 (BeAn 4116/4073). Structure prediction originates from UNAFold Web Server and supplementary graphics added at Biorender.com (https://BioRender.com/2kr46w4).

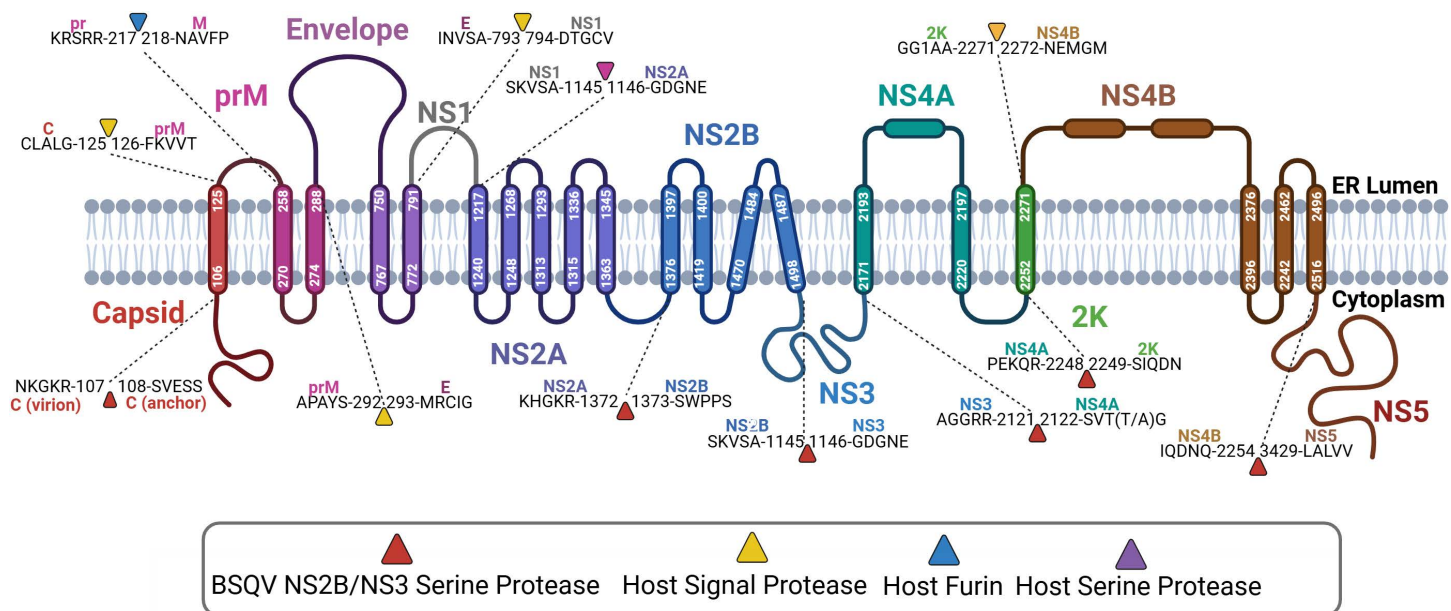https://doi.org/10.1371/journal.pntd.0013774.g004

Domain II also contains structure duplication patterns that vary across orthoflavivirus clades; MB species generally contain 1–2 DBs [67,72]. The BSQV strains differ by two mutations (10641 and 10643) within the DB-II structure (Fig 4). Short direct repeat sequences (CS/RCS) are conserved 3'UTR motifs that cluster primarily within Domain II DBs [73–75] and help maintain efficient rates of RNA synthesis [73], alongside proposed roles in vector-vertebrate transmission [76,77]. Sequence alignment revealed putative BSQV sequences for RCS2 and CS1 on DB I and II, respectively, with CS2 partially straddling the sHP.

Domain III is the most conserved domain. Structural motifs include the short hairpin structure (shP) and the 3'SL with roles in viral replication and viability, alongside interactions with viral and host cell factors [47,66,78,79]. The top of the BSQV 3'SL displays a conserved 5′-CACAG-3′ pentanucleotide motif (Fig 4); a major determinant for orthoflavivirus replication [80–82].

Open reading frame. A brief overview of the notable features of the three structural (capsid, pr/M, envelope) and seven nonstructural (NS1, NS2A, NS2B, NS3, NS4A, NS4B, NS5) of BSQV (Fig 5) is described below. BSQV genome annotation across strains (polypeptide boundaries, predicted PTM sites, amino acid differences) is available in S3 Table. Predicted post-translational modifications by gene are listed in Table 4.

Capsid. The orthoflavivirus capsid protein is a critical structural component for RNA packaging and virion assembly [84]. The BSQV capsid protein is 126 amino acids long, composed of 107 amino acids at the N-terminus as the core capsid protein, followed by eighteen amino acids residues at the C-terminus functioning as a transmembrane domain (TMD) anchor. There is one sequence variation between BeAn 217201 versus BeAn 4116 and BeAn4073. There are

Adapted from *Plante et al 2023*

Fig 5. BSQV Polyprotein Annotation. Consensus amino acid sequence across the three BSQV strains. The three nonstructural and seven structural proteins are distinguished by chain color. Polyprotein cleavage sites with the five preceding and five successive residues are defined, with associated proteases distinguished by triangle color. Figure adapted from Plante et al. [83] and created at Biorender.com (https://BioRender.com/jo332fm).

https://doi.org/10.1371/journal.pntd.0013774.g005

three predicted phosphorylation sites, including the first residue in the TMD and two residues within the cytoplasmic domain.

prM/M. Final orthoflavivirus virion maturation occurs in the trans-Golgi network upon furin cleavage of prM [85]. The BSQV prM protein is 157 amino acids long, with a pr peptide of 92 amino acids and an M peptide at the C-terminus with 77 amino acids that spans two predicted TMDs. There is only one sequence variation between BeAn 217201 (threonine) differs from BeAn 4116 and BeAn 4073 (isoleucine). Phosphorylation is predicted at six residues, with only the last site internal to the mature M protein segment. Two N-linked glycosylation sites, one per the pr and M portions, were predicted *in silico* (S3 Table). Six conserved cysteine residues, contributing to structural integrity via intramolecular disulfide bond formation [39,86], aligned to the pr region of BSQV and other orthoflaviviruses in our genus-wide multiple sequence alignment (see data repository).

Envelope. The envelope protein composes the external surface of the virion and enables initial viral fusion with the host cell membrane to initiate infection [87,88]. The BSQV envelope protein is 501 amino acids long, with two predicted TMDs, and five variable residues. Phosphorylation was predicted at twenty-one residues. All BSQV strains share the twelve strictly conserved orthoflavivirus cysteine residues [89]. Residue N154 is a common glycosylation site across orthoflaviviruses that contributes to target host cell attachment, virion assembly and secretion, and pathogenesis [90,91]; this site was predicted, albeit with low confidence, only in the BeAn 217201 strain.

NS1. The NS1 protein plays multiple roles in genome replication and virion maturation, complement activation and signal transduction, immune stimulation, host immune evasion, and pathogenesis [92–95]. The BSQV NS1 protein is 352

Table 4. Predicted BSQV Polyprotein Posttranslational Modifications.

Gene	Phosphorylation	Glycosylation	Cysteine	Variable Residues
Capsid	T101			BeAn 217201
	S91 (BeAn4116, BeAn 4073)			91: S --> N
	S108			
prM	T15	N31	C34	BeAn 217201
	T82	N148	C45	86: I --> T
	T86 (BeAn 217201)		C53	
	T90		C67	
	S85		C69	
	S147		C81	
Envelope	T32	N154 (BeAn 217201)	C295	BeAn 217201
	T97 (BeAn4116, BeAn 4073)	N498	C322	93: R --> K
	T115 (BeAn 4073)		C352	BeAn 4116
	T247		C366	154: N --> S
	T310		C384	BeAn 4073
	T320		C397	120: E --> K
	T365		C408	143: I --> V
	S142		C413	156: S --> L
	S153,		C481	
	S156 (BeAn 4116)		C582	
	S172		C599	
	S174		C630"	
	S178			
	S193			
	S209			
	S230			
	S276			
	Y137			
	Y182			
	Y379			
	Y383			
NS1	T2	N207*	C797	BeAn 217201
	T87		C808	175: M --> I
	T344		C848	
	S45		C936	
	S127		C972	
	S139		C1016	
	S297		C1073	
	S300		C1084	
	S304		C1105	
	S339		C1106	
	S351		C1109	
	Y32		C1122	
	Y113			

(Continued)

Table 4. (Continued)

Gene	Phosphorylation	Glycosylation	Cysteine	Variable Residues
NS2A	T50	N131*		BeAn 217201
	T100	N210		202: T -->A
	T169			205: Q -->H
	S185			
	S197			
NS2B	S1			
	S5			
	S61			
	S69			
	S72			
	S86			
	S128			
NS3	T112			BeAn 217201
	T175			88: R -->H
	T184			109: V -->I
	T201			210: Q -->K
	T245			347: T -->A
	T267			
	T377			
	T393			
	S17			
	S251			
	S253			
	S306			
	S426			
	S547			
	S585			
	S596			
	Y473			
NS4A	S1			BeAn 217201
	S127			4: T -->A
				93: G -->V
NS4B	T20			
	T250			
	S24			
	S88			
	S193			

(Continued)

Table 4. (Continued)

Gene	Phosphorylation	Glycosylation	Cysteine	Variable Residues
NS5	T93	N233		BeAn 217201
	T161			197: L -->M
	T266 (BeAn 217201)			266: I -->T
	T395			383: R -->K
	T421			563: Q -->K
	T543			644: H -->L
	T572			810: N -->T
	T640			897: g -->E
	T751			
	T794			
	T862			
	S56			
	S59			
	S128			
	S214			
	S319			
	S340			
	S342			
	S386			
	S499,			
	S523			
	S595			
	S633			
	S665			
	S745			
	Y22			
	Y27			
	Y504			
	Y883			

Putative phosphorylation and N-linked glycosylation sites based on *in silico* predictions, and cysteine residues involved in disulfide bond formation, for each gene in the BSQV polypeptide. Variable residue positions are noted, internal to gene, with arrow pointing to variation in specified strain (2nd amino acid) compared to other two strains (1st amino acid). PTM predictions are matched across the three BSQV strains, otherwise indicated by a specific strain within parentheses. * - indicates high confidence for predicted glycosylation site with 8/9 or 9/9 jury agreement.

amino acids long without predicted TMDs. There is one variable residue between BeAn 217201 versus BeAn 4116 and BeAn 4073. A single BSQV NS1 residue had a positive glycosylation prediction, with high confidence, that matched one of two conserved orthoflavivirus glycosylation sites that are critical for NS1 secretion, viral replication, immunogenicity, ER remodeling activity, and neurovirulence [26,92,95–97]; however, only one site had a positive prediction with high confidence. All BSQV strains have thirteen predicted phosphorylation sites, including a match (Y32) to one of two predicted NS1 phosphorylation sites essential for DENV propagation [98]. The twelve conserved cysteine residues [93] aligned between all BSQV strains and other orthoflavivirus species.

NS2A. The NS2A protein promotes RNA synthesis, virion assembly, immune evasion, and pathogenesis [36,37,99–104]. The BSQV NS2A protein is 227 amino acids long with two variable residues and five predicted TMDs. BeAn217201 differs from BeAn 4116 and BeAn 4073 at two residues. Phosphorylation was predicted for the same five sites across

all three BSQV strains. Glycosylation was predicted at two residues, one with high confidence by total jury agreement; however, validation or functional analysis of N-linked glycosylation of the NS2A protein has not been reported for other orthoflaviviruses.

NS2B. The NS2B is a critical cofactor for the NS3 viral serine protease, alongside roles in viral RNA synthesis, virion assembly, and host immune evasion [28,32,105]. The BSQV NS2B protein is 131 amino acids long with no variable residues and has a predicted 51 amino acid hydrophilic cytoplasmic domain central to its four TMDs. Phosphorylation was predicted for the same seven residues across all three BSQV strains. No N-linked glycosylation sites in the NS2B protein were predicted *in silico*.

NS3. The NS3 protein functions as both a serine protease and a NTPase/helicase, with critical roles in RNA replication and RNA strand synthesis [24,106,107]. The BSQV NS3 protein is 618 amino acids, lacks TMDs, and has four variable residues across strains. Phosphorylation was predicted at seventeen residues. No glycosylation sites in the NS3 protein were predicted *in silico*.

NS4A and 2K. The NS4A protein is critical for viral replication and cellular membrane remodeling via 2K protein dependent mechanisms [33,108,109]. NS4A also contributes to immune evasion with proposed contributions for persistent orthoflavivirus infections [108,110]. The BSQV NS4A protein is 127 amino acids long and is tailed at the C-terminal by 23 transmembrane residues composing the 2K peptide. Two variable residues between BeAn 217201 versus BeAn 4116 and BeAn 4073 are present in the NS4A region. There are no variable residues in the 2K domain. One phosphorylation site was predicted at each peptide's first amino acid (serine). No glycosylation sites in NS4A or 2K were predicted *in silico*.

NS4B. Via an interplay of direct interactions with other nonstructural proteins, the NS4B protein plays roles in membrane remodeling, innate immune evasion, and potentially, coordinating ER-Golgi trafficking of immature virions [35,111,112]. The BSQV NS4B protein is 253 amino acids long with three TMDs and lacking variable residues. Phosphorylation was predicted at the same five sites for each BSQV strain. No N-linked glycosylation sites were positively predicted *in silico.*

NS5. The NS5 functions as a methyltransferase responsible for genome capping, as well as a RNA-dependent RNA polymerase with roles in viral replication alongside contributions to the innate immune response [113]. The BSQV NS5 protein is 905 amino acids long with 7 variable residues between BeAn 217201 versus BeAn 4116 and BeAn 4073. Orthoflavivirus NS5 phosphorylation is recognized but minimally understood [114]. Phosphorylation was predicted at twenty-nine residues in BSQV NS5. One N-linked glycosylation site was predicted *in silico*; however, N-linked glycosylation of the NS5 protein is not reported for other orthoflaviviruses.

Replication kinetics

BSQV replicated robustly in all ten vertebrate cell lines, including the four human cell lines (Fig 6), with peak titers (6.5 - 8.3 $\log_{10}$ PFU/mL) at approximately 3 dpi (S4 Table). BSQV reached similarly high titers in C6/36 and C7-10 (5.6-7.7 $\log_{10}$ PFU/mL) [115,116] cells, which are *Ae. albopictus* cell lines that lack a functional RNAi pathway. Contrastingly, BSQV replicated poorly in Aag2 (*Ae. aegypti*) (peak titer: 1.4 $\log_{10}$ PFU/mL) and U4.4 (*Ae. albopictus*) (peak titer: 2.86 $\log_{10}$ PFU/mL) which are both RNAi-competent *Aedes* lines [116–118]. This variation in replication is not entirely attributable to RNAi since the virus replicated to high titers in RNAi-competent cells from *Cx. tarsalis* and *Cx. quinquefasciatus* (CT, HSU,CxTr) [118–120]. Overall, productive BSQV replication in the three *Culex* cell lines corroborates the competence bias of *Culex* suggested by field collections [2], while *Aedes* competence remains to be determined, with no reported BSQV isolations from *Aedes* species or confirmatory *in vivo* studies.

Sustained peak viral titer corresponded with cell viability, with peak titer plateaus in susceptible mosquito lines and post-peak declines in vertebrate cells. CPE in mosquito cells, particularly clumping, was attributed to cell overgrowth conditions (S1 File). The lack of mosquito cell ablation correlates to natural arbovirus transmission dynamics that rely on persistent infection and innate immune tolerance in vector species [121–123]. Six vertebrate cell lines had near total (>95%)
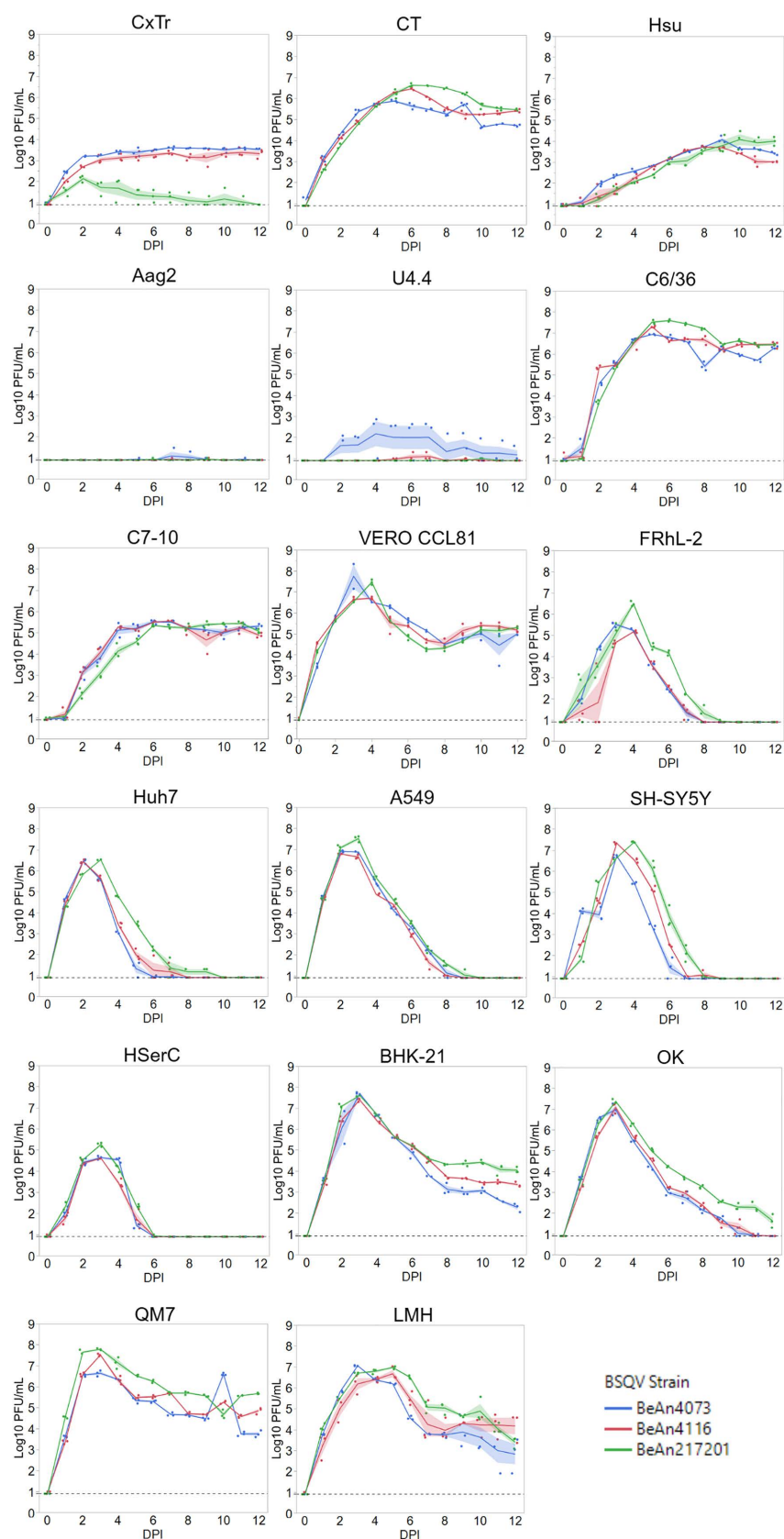
Fig 6. Replication kinetics. Kinetic curves of each BSQV strain in mosquito and vertebrate cell lines. Each data point represents the daily mean of three independent replicate wells per BSQV strain per cell line. Dotted lines represent the lower limit of detection (0.09 $\log_{10}$ PFU/mL); data points with no detectable BSQV are represented at the lower limit of detection. BSQV strains are represented by line color, with colored error bands indicating standard error of the mean by dpi.

monolayer ablation: BHK-21, Huh7, OK, Vero CCL81, SH-SY5Y, and LMH, in contrast to four cell lines with either minimal (<5%) (FRhL-2, HSerC) or partial (~50%) (A549, QM7) ablation at endpoint (S1 File). The curtailed CPE in human testicular and lung cells, compared to the extensive destruction of neuroblastoma and liver cells, lends premise for BSQV tissue tropisms, in line with observed liver, brain, and kidney BSQV pathologies in surveillance or laboratory animals [1,5]. SH-SY5Y and HSerC susceptibility need to be considered in context of the blood-brain-barrier and the blood-testis barrier. The capacity of BSQV to cross either of these barriers, as ZIKV does [124,125], in immunologically intact vertebrates remains unknown.

BeAn 217201, BeAn 4116, and BeAn 4073 infection did not produce any observable CPE differences per each cell line. The initial two-way repeated measures ANOVA defined a significant interaction between day post infection and virus strain ($p = 0.00000$-0.00075) in all cell lines, indicating significant differences in replication dynamics between strains, except for Aag2 cells ($p = 0.67833$) which had daily titers (0-1.48 $\log_{10}$ PFU/mL) typically below LOD (S4 Table). Post-hoc tests (Tukey connected letter display) delineated specific intra-strain differences in daily viral titer across all cell lines, except Aag2 and U4.4 (S5 Table). Peak BSQV titers were significantly different for each mosquito cell line. For vertebrates, HSerC supported the significantly lowest peak BSQV titers over the 12-day time course. QM7, Vero, SH-SY5Y, OK, A549, and BHK-21 and/or LMH had similar overall peak BSQV titers but demonstrated strain differences with BeAn 217201 having significantly higher peak titers compared to the similar peaks of BeAn 4116 and BeAn 4073, albeit the magnitude of differences in viral titer were small (max difference = 1.6 $\log_{10}$ PFU/ml, 2dpi FRhL-2). Across mosquito and vertebrate cells, BeAn 4073 typically reached peak and/or plateau titers first, whereas BeAn 217201 commonly lagged by one or more days. Future BSQV characterization will benefit from *in vivo* models that investigate these suggested phenotypic differences across strains. Overall, these *in vitro* replication kinetics patterns indicate that BSQV is capable of opportunistic host-range expansion during contact interactions between sylvatic, epizootic, and urban vector-host species.

Conclusions

We demonstrated that three historical BSQV isolates (BeAn217201, BeAn 4116, BeAn 4073) exhibit the canonical orthoflavivirus characteristics including (i) size and icosahedral morphology, (ii) virion trafficking and host membrane remodeling in mosquito and vertebrate cells, (iii) *Orthoflavivirus* evolutionary relationships, and (iv) genome size and architecture with conserved sequence and structural motifs, and generalized PTM patterns [13,62,126–128]. In addition, BSQV infection was robust across diverse mosquito (peridomestic and urban species) and vertebrate (avian, nonhuman primate, rodent, marsupial, human) cell lines, with notable exceptions potentially related to innate immunity intactness (RNAi, interferon) or mosquito genus (*Culex, Aedes*). Overall, our data support conclusions from historical surveillance that BSQV is a *Culex*-vectored orthoflavivirus with a broad vertebrate and vector range, including species living in proximity to urban communities, suggesting the potential to infect and cause disease in humans.

The limitations of our study include usage of a restricted subset of representative mosquito and vertebrate cell lines to extrapolate a broad vector-host susceptibility. Orthoflavivirus exploitation of PTM machinery is critical to the viral life cycle (142,145–148); our PTM predictions were conducted based primarily on publicly-accessibility of online software tools and thus were not exhaustive. We were only able to investigate the BSQV genome and viral fitness using three available isolates, thereby limiting in-depth genomic meta-analyses of conserved and divergent motifs across strains. Furthermore, BeAn 4073 and BeAn 4116 isolates originated from the same sentinel monkey, via blood collections occurring three days apart [1]. However, BeAn 4073 and BeAn 4116 phenotypic differences cannot be discounted since (i) viral passage

histories differ with additional SM passaging for BeAn 4073 and thus greater potential for murine host adaptation, (ii) consensus sequences from the two viruses have four divergent residues in the Domain I of the envelope protein, and (iii) the two viruses show significant variation in replication kinetics in multiple cell lines. Overall, the precise sequence and structure requirements of predicted sequence, structure, or PTM sites, or the impact of strain differences, towards BSQV replication, translation, pathogenesis, or immune evasion, remain unknown. Lastly, cell line susceptibility does not directly connote transmission potential because: (a) many of the insect cell lines originated from larval stages, and (b) replication kinetics do not reflect host viremia or vector competence outcomes in the context of organismal-level physical barriers or immune factors. Future *in vivo* pathogenesis and transmission studies can enable correlations of BSQV phenotype to genomic annotation data as well as assess capacity of BSQV to sustain urban transmission cycles beyond sporadic spill-over via opportunistic exploitation. Many foundational research studies for neglected orthoflaviviruses coincide with their unprecedented emergence [7,9,11,14,129]. Proactive characterization of arboviruses species like BSQV can be leveraged to facilitate public health response, clinical management, and countermeasure development to combat future emergence scenarios.

Supporting information

S1 File. Replication Kinetics - Cytopathic Effects.
(PDF)

S1 Table. Orthoflavivirus Genome Sequences Phylogeny. List of flavivirus sequences used for phylogenetic analysis. Details include accession number, virus abbreviation, strain name, sequence length (nucleotides), location and year of isolation. Subclades are listed as: mosquito-borne (MB), tick-borne (TB), insect specific (IS), or no known vector (NKV).
(XLSX)

S2 Table. Predicted cyclization and conserved sequence motifs in BSQV UTR. Predicted RNA nucleotide sequences of (i) complementary UAR, DAR, and CS motifs in the BSQV 5' and 3' genomic termini, and (ii) and conserved orthoflavivirus CS/RCS and penta-nucleotide in the 3' UTR. Lowercase letters indicate a nucleotide with a noncomplementary pairing. *Extension into capsid protein cds.
(XLSX)

S3 Table. Genome Annotation - Identification of UTR and polypeptide boundaries and sequences for BeAn217201, BeAn 4116, BeAn 4073, and CoAr41922. Software prediction results for glycosylation and phosphorylation sites in the open reading frames of BeAn217201, BeAn 4116, and BeAn 4073.
(XLSX)

S4 Table. Replication Kinetics – Titration Data – Table of individual log titers for each BSQV strain and replicate wells 0–12 dpi in all mosquito (n = 7) and vertebrate (n = 10) cell lines. Table of peak log titer for each replicate per BSQV strain per cell line over kinetics time course.
(XLSX)

S5 Table. Replication Kinetics – Statistics - Two-Way RM ANOVA and Tukey-Kramer post-hoc test results of replication kinetics studies analyzing effects on viral titer by day post-infection, strain, and the interaction between day and strain. One-Way ANOVA and Tukey-Kramer post-hoc test results of replication kinetics studies analyzing effects on peak viral titer by cell line and strain, with vertebrate and mosquito cell lines considered as individual groups. Connecting letter display tables color coded to indicate group with non-significant difference in daily or peak viral titers.
(XLSX)

Acknowledgments

Author contributions

References

1. Gomes G, Causey OR. Bussuquara, a new arthropod-borne virus. Proc Soc Exp Biol Med. 1959;101(2):275–9.

2. Steck MR, Buenemann M, Vasilakis N. Bussuquara Virus: A Neglected Orthoflavivirus with Broad Distribution Across Central and South America and the Caribbean. Viruses. 2025;17(2):183. https://doi.org/10.3390/v17020183 PMID: 40006938

3. Srihongse S, Johnson CM. The first isolation of bussuquara virus from man. Trans R Soc Trop Med Hyg. 1971;65(4):541–2.

4. Glowacki G, Spinsanti L, Basualdo MA, Díaz G, Contigiani M. Prevalence of Flavivirus antibodies in young voluntary recruits to military service in the province of Formosa, Argentina. Rev Argent Microbiol. 1998;30(4):170–5. PMID: 9950038

5. de Paola D, Bruno-Lobo GG, Bruno-Lobo M. Immunofluorescence in pathogenesis of group A, B, and C arbovirus in the hamster. An Microbiol (Rio J). 1968;15:35–51. PMID: 4913570

6. Faria NR, Azevedo R do S da S, Kraemer MUG, Souza R, Cunha MS, Hill SC, et al. Zika virus in the Americas: Early epidemiological and genetic findings. Science. 2016;352(6283):345–9. https://doi.org/10.1126/science.aaf5036 PMID: 27013429

7. Dengue outbreaks in Brazil and Latin America: the new and continuing challenges. Int J Infect Dis. 2024;147:107192.

8. Beltz LA. Chapter 8 - Other Neglected Mosquito-Borne Flaviviruses: Ilhéus, Bussuquara, Rocio, Kokobera, Stratford, and Wesselsbron Viruses. In: Beltz LA, editor. Zika and Other Neglected and Emerging Flaviviruses [Internet]. Elsevier; 2021 [cited 2023 May 24]. p. 115–25. Available from: https://www.sciencedirect.com/science/article/pii/B9780323825016000104

9. da Costa VG, Saivish MV, Lino NAB, Bittar C, de Freitas Calmon M, Nogueira ML, et al. Clinical Landscape and Rate of Exposure to Ilheus Virus: Insights from Systematic Review and Meta-Analysis. Viruses. 2022;15(1):92. https://doi.org/10.3390/v15010092 PMID: 36680131

10. Gianchecchi E, Cianchi V, Torelli A, Montomoli E. Yellow Fever: Origin, Epidemiology, Preventive Strategies and Future Prospects. Vaccines. 2022;10(3):372. https://doi.org/10.3390/vaccines10030372

11. Saivish MV, Gomes da Costa V, de Lima Menezes G, Alves da Silva R, Dutra da Silva GC, Moreli ML. Rocio Virus: An Updated View on an Elusive Flavivirus. Viruses. 2021;13(11):2293. https://doi.org/10.3390/v13112293

12. Dye-Braumuller KC, Prisco RA, Nolan MS. (Re)Emerging Arboviruses of Public Health Significance in the Brazilian Amazon. Microorganisms. 2025;13(3):650. https://doi.org/10.3390/microorganisms13030650 PMID: 40142542

13. Pierson TC, Diamond MS. The continued threat of emerging flaviviruses. Nat Microbiol. 2020;5(6):796–812. https://doi.org/10.1038/s41564-020-0714-0 PMID: 32367055

14. Leung C. A lesson learnt from the emergence of Zika virus: What flaviviruses can trigger Guillain-Barré syndrome? J Med Virol. 2020;92(12):2938–45. https://doi.org/10.1002/jmv.25717 PMID: 32077499

15. Cunha MS, Costa PAG, Correa IA, de Souza MRM, Calil PT, da Silva GPD, et al. Chikungunya Virus: An Emergent Arbovirus to the South American Continent and a Continuous Threat to the World. Front Microbiol [Internet]. 2020 [cited 2024 Apr 3];11. Available from: https://www.ncbi.nlm.nih.gov/pmc/articles/PMC7332961/

16. Murray KO, Mertens E, Despres P. West Nile virus and its emergence in the United States of America. Vet Res. 2010;41(6):67. https://doi.org/10.1051/vetres/2010039 PMID: 21188801

17. Arbovirus Catalog - CDC Division of Vector-Borne Diseases (DVBD) [Internet]. [cited 2024 Jan 24]. Available from: https://wwwn.cdc.gov/arbocat/

18. Schirtzinger EE, Jasperson DC, Swanson DA, Mitzel D, Drolet BS, Richt JA. Establishment of a Culex tarsalis (Diptera: Culicidae) cell line and its permissiveness to arbovirus infection. J Med Entomol. 2022;60(1):239–44.

19. Rio DC, Ares M Jr, Hannon GJ, Nilsen TW. Purification of RNA using TRIzol (TRI reagent). Cold Spring Harb Protoc. 2010;2010(6):pdb.prot5439. https://doi.org/10.1101/pdb.prot5439 PMID: 20516177

20. Bolger AM, Lohse M, Usadel B. Trimmomatic: a flexible trimmer for Illumina sequence data. Bioinformatics. 2014;30(15):2114–20.

21. Li W, Godzik A. Cd-hit: a fast program for clustering and comparing large sets of protein or nucleotide sequences. Bioinformatics. 2006;22(13):1658–9. https://doi.org/10.1093/bioinformatics/btl158

22. LoFreq: a sequence-quality aware, ultra-sensitive variant caller for uncovering cell-population heterogeneity from high-throughput sequencing datasets | Nucleic Acids Research | Oxford Academic [Internet]. [cited 2025 Jun 28]. Available from: https://academic.oup.com/nar/article/40/22/11189/1152727

23. Fast gapped-read alignment with Bowtie 2 | Nature Methods [Internet]. [cited 2024 Aug 5]. Available from: https://www.nature.com/articles/nmeth.1923

24. Shiryaev SA, Strongin AY. Structural and functional parameters of the flaviviral protease: a promising antiviral drug target. Future Virol. 2010;5(5):593–606. https://doi.org/10.2217/fvl.10.39 PMID: 21076642

25. Tsu BV, Fay EJ, Nguyen KT, Corley MR, Hosuru B, Dominguez VA, et al. Running with scissors: evolutionary conflicts between viral proteases and the host immune system. Front Immunol. 2021;12. https://doi.org/10.3389/fimmu.2021.769543

26. van den Elsen K, Quek JP, Luo D. Molecular Insights into the Flavivirus Replication Complex. Viruses. 2021;13(6):956. https://doi.org/10.3390/v13060956 PMID: 34064113

27. Ci Y, Shi L. Compartmentalized replication organelle of flavivirus at the ER and the factors involved. Cell Mol Life Sci. 2021;78(11).

28. Wahaab A, Mustafa BE, Hameed M, Stevenson NJ, Anwar MN, Liu K, et al. Potential Role of Flavivirus NS2B-NS3 Proteases in Viral Pathogenesis and Anti-flavivirus Drug Discovery Employing Animal Cells and Models: A Review. Viruses. 2021;14(1):44. https://doi.org/10.3390/v14010044 PMID: 35062249

29. Rothan HA, Kumar M. Role of Endoplasmic Reticulum-Associated Proteins in Flavivirus Replication and Assembly Complexes. Pathogens. 2019;8(3):148. https://doi.org/10.3390/pathogens8030148 PMID: 31547236

30. Verhaegen M, Vermeire K. The endoplasmic reticulum (ER): a crucial cellular hub in flavivirus infection and potential target site for antiviral interventions. Npj Viruses. 2024;2(1):24. https://doi.org/10.1038/s44298-024-00031-7 PMID: 40295816

31. Blazevic J, Rouha H, Bradt V, Heinz FX, Stiasny K. Membrane anchors of the structural flavivirus proteins and their role in virus assembly. J Virol. 2016;90(14):6365–78. https://doi.org/10.1128/JVI.00456-16

32. Li XD, Deng CL, Ye HQ, Zhang HL, Zhang QY, Chen DD. Transmembrane Domains of NS2B Contribute to both Viral RNA Replication and Particle Formation in Japanese Encephalitis Virus. J Virol. 2016;90(12):5735–49.

33. Miller S, Kastner S, Krijnse-Locker J, Bühler S, Bartenschlager R. The non-structural protein 4A of dengue virus is an integral membrane protein inducing membrane alterations in a 2K-regulated manner. J Biol Chem. 2007;282(12):8873–82. https://doi.org/10.1074/jbc.M609919200 PMID: 17276984

34. Rana J, Slon Campos JL, Leccese G, Francolini M, Bestagno M, Poggianella M, et al. Role of Capsid Anchor in the Morphogenesis of Zika Virus. J Virol. 2018;92(22):e01174-18. https://doi.org/10.1128/JVI.01174-18 PMID: 30158295

35. Zmurko J, Neyts J, Dallmeier K. Flaviviral NS4b, chameleon and jack-in-the-box roles in viral replication and pathogenesis, and a molecular target for antiviral intervention. Rev Med Virol. 2015;25(4):205–23. https://doi.org/10.1002/rmv.1835 PMID: 25828437

36. Xie X, Zou J, Puttikhunt C, Yuan Z, Shi PY. Two distinct sets of NS2A molecules are responsible for dengue virus RNA synthesis and virion assembly. J Virol. 2014;89(2):1298–313. https://doi.org/10.1128/JVI.02245-14

37. Xie X, Gayen S, Kang C, Yuan Z, Shi PY. Membrane topology and function of dengue virus NS2A protein. J Virol. 2013;87(8):4609–22.

38. Wicker JA, Whiteman MC, Beasley DWC, Davis CT, McGee CE, Lee JC, et al. Mutational analysis of the West Nile virus NS4B protein. Virology. 2012;426(1):22–33. https://doi.org/10.1016/j.virol.2011.11.022 PMID: 22314017

39. Nowak T, Wengler G. Analysis of disulfides present in the membrane proteins of the West Nile flavivirus. Virology. 1987;156(1):127–37. https://doi.org/10.1016/0042-6822(87)90443-0 PMID: 3811228

40. Blitvich BJ, Scanlon D, Shiell BJ, Mackenzie JS, Pham K, Hall RA. Determination of the intramolecular disulfide bond arrangement and biochemical identification of the glycosylation sites of the nonstructural protein NS1 of Murray Valley encephalitis virus. J Gen Virol. 2001;82(9):2251–6.

41. Zuker M. Mfold web server for nucleic acid folding and hybridization prediction. Nucl Acids Res. 2003;31(13):3406.

42. Li XD, Deng CL, Yuan ZM, Ye HQ, Zhang B. Different degrees of 5'-to-3' DAR interactions modulate Zika virus genome cyclization and host-specific replication. J Virol. 2020;94(5):e01602-19. https://doi.org/10.1128/JVI.01602-19

43. Alvarez DE, Lodeiro MF, Ludueña SJ, Pietrasanta LI, Gamarnik AV. Long-range RNA-RNA interactions circularize the dengue virus genome. J Virol. 2005;79(11):6631–43. https://doi.org/10.1128/JVI.79.11.6631-6643.2005 PMID: 15890901

44. Hahn CS, Hahn YS, Rice CM, Lee E, Dalgarno L, Strauss EG. Conserved elements in the 3′ untranslated region of flavivirus RNAs and potential cyclization sequences. J Mol Biol. 1987;198(1):33–41.

45. Zhang B, Dong H, Stein DA, Iversen PL, Shi P-Y. West Nile virus genome cyclization and RNA replication require two pairs of long-distance RNA interactions. Virology. 2008;373(1):1–13. https://doi.org/10.1016/j.virol.2008.01.016 PMID: 18258275

46. Mrozowich T, Park SM, Waldl M, Henrickson A, Tersteeg S, Nelson CR, et al. Investigating RNA-RNA interactions through computational and biophysical analysis. Nucleic Acids Res. 2023;51(9):4588–601. https://doi.org/10.1093/nar/gkad223 PMID: 36999609

47. Villordo SM, Gamarnik AV. Genome cyclization as strategy for flavivirus RNA replication. Virus Res. 2009;139(2):230–9. https://doi.org/10.1016/j.virusres.2008.07.016 PMID: 18703097

48. Khromykh AA, Meka H, Guyatt KJ, Westaway EG. Essential role of cyclization sequences in flavivirus RNA replication. J Virol. 2001;75(14):6719–28. https://doi.org/10.1128/JVI.75.14.6719-6728.2001 PMID: 11413342

49. Khromykh AA, Kondratieva N, Sgro J-Y, Palmenberg A, Westaway EG. Significance in replication of the terminal nucleotides of the flavivirus genome. J Virol. 2003;77(19):10623–9. https://doi.org/10.1128/jvi.77.19.10623-10629.2003 PMID: 12970446

50. Friebe P, Shi P-Y, Harris E. The 5' and 3' downstream AUG region elements are required for mosquito-borne flavivirus RNA replication. J Virol. 2011;85(4):1900–5. https://doi.org/10.1128/JVI.02037-10 PMID: 21123391

51. Roundy CM, Azar SR, Rossi SL, Weaver SC, Vasilakis N. Insect-Specific Viruses: A Historical Overview and Recent Developments. Adv Virus Res. 2017;98:119–46.

52. Blitvich BJ, Firth AE. Insect-specific flaviviruses: a systematic review of their discovery, host range, mode of transmission, superinfection exclusion potential and genomic organization. Viruses. 2015;7(4):1927–59. https://doi.org/10.3390/v7041927 PMID: 25866904

53. Auguste AJ, Adams AP, Arrigo NC, Martinez R, Travassos da Rosa APA, Adesiyun AA. Isolation and characterization of sylvatic mosquito-borne viruses in Trinidad: enzootic transmission and a new potential vector of mucambo virus. Am J Trop Med Hyg. 2010;83(6):1262–5.

54. Guzman H, Contreras-Gutierrez MA, Travassos da Rosa APA, Nunes MRT, Cardoso JF, Popov VL, et al. Characterization of Three New Insect-Specific Flaviviruses: Their Relationship to the Mosquito-Borne Flavivirus Pathogens. Am J Trop Med Hyg. 2018;98(2):410–9. https://doi.org/10.4269/ajtmh.17-0350 PMID: 29016330

55. de Figueiredo MLG, Amarilla AA, de Figueiredo GG, Alfonso HL, Lippi V, Maia FGM, et al. Cacipacore virus as an emergent mosquito-borne Flavivirus. Rev Soc Bras Med Trop. 2017;50(4):539–42. https://doi.org/10.1590/0037-8682-0485-2016 PMID: 28954077

56. Carrera J-P, Guzman H, Beltrán D, Díaz Y, López-Vergès S, Torres-Cosme R, et al. Mercadeo Virus: A Novel Mosquito-Specific Flavivirus from Panama. Am J Trop Med Hyg. 2015;93(5):1014–9. https://doi.org/10.4269/ajtmh.15-0117 PMID: 26304915

57. Katoh K, Standley DM. MAFFT multiple sequence alignment software version 7: improvements in performance and usability. Mol Biol Evol. 2013;30(4):772–80.

58. Minh BQ, Schmidt HA, Chernomor O, Schrempf D, Woodhams MD, von Haeseler A. IQ-TREE 2: New Models and Efficient Methods for Phylogenetic Inference in the Genomic Era. Mol Biol Evol. 2020;37(5):1530–4. https://doi.org/10.1093/molbev/msaa015

59. Kalyaanamoorthy S, Minh BQ, Wong TKF, von Haeseler A, Jermiin LS. ModelFinder: fast model selection for accurate phylogenetic estimates. Nat Methods. 2017;14(6):587–9. https://doi.org/10.1038/nmeth.4285 PMID: 28481363

60. Hoang DT, Chernomor O, von Haeseler A, Minh BQ, Vinh LS. UFBoot2: Improving the Ultrafast Bootstrap Approximation. Mol Biol Evol. 2018;35(2):518–22.

61. Guindon S, Dufayard JF, Lefort V, Anisimova M, Hordijk W, Gascuel O. New algorithms and methods to estimate maximum-likelihood phylogenies: assessing the performance of PhyML 3.0. Syst Biol. 2010;59(3):307–21.

62. Genus: Orthoflavivirus | ICTV [Internet]. [cited 2025 May 11]. Available from: https://ictv.global/report/chapter/flaviviridae/flaviviridae/orthoflavivirus

63. Ng WC, Soto-Acosta R, Bradrick SS, Garcia-Blanco MA, Ooi EE. The 5' and 3' Untranslated Regions of the Flaviviral Genome. Viruses. 2017;9(6):137. https://doi.org/10.3390/v9060137 PMID: 28587300

64. Gebhard LG, Filomatori CV, Gamarnik AV. Functional RNA elements in the dengue virus genome. Viruses. 2011;3(9):1739–56. https://doi.org/10.3390/v3091739 PMID: 21994804

65. Mishra B, Aduri R. The RNA Secondary Structure Analysis Reveals Potential for Emergence of Pathogenic Flaviviruses. Food Environ Virol. 2022;14(1):10–29. https://doi.org/10.1007/s12560-021-09502-z PMID: 34694573

66. Fernández-Sanlés A, Ríos-Marco P, Romero-López C, Berzal-Herranz A. Functional Information Stored in the Conserved Structural RNA Domains of Flavivirus Genomes. Front Microbiol. 2017;8:546. https://doi.org/10.3389/fmicb.2017.00546 PMID: 28421048

67. Ramos-Lorente S, Romero-López C, Berzal-Herranz A. Information Encoded by the Flavivirus Genomes beyond the Nucleotide Sequence. Int J Mol Sci. 2021;22(7):3738. https://doi.org/10.3390/ijms22073738 PMID: 33916729

68. De Falco L, Silva NM, Santos NC, Huber RG, Martins IC. The Pseudo-Circular Genomes of Flaviviruses: Structures, Mechanisms, and Functions of Circularization. Cells. 2021;10(3):642. https://doi.org/10.3390/cells10030642 PMID: 33805761

69. Zeng M, Duan Y, Zhang W, Wang M, Jia R, Zhu D, et al. Universal RNA Secondary Structure Insight Into Mosquito-Borne Flavivirus (MBFV) cis-Acting RNA Biology. Front Microbiol [Internet]. 2020 [cited 2025 Apr 17];11. Available from: https://www.frontiersin.org https://www.frontiersin.org/journals/microbiology/articles/10.3389/fmicb.2020.00473/full

70. Villordo SM, Filomatori CV, Sánchez-Vargas I, Blair CD, Gamarnik AV. Dengue virus RNA structure specialization facilitates host adaptation. PLoS Pathog. 2015;11(1):e1004604. https://doi.org/10.1371/journal.ppat.1004604 PMID: 25635835

71. Kieft JS, Rabe JL, Chapman EG. New hypotheses derived from the structure of a flaviviral Xrn1-resistant RNA: Conservation, folding, and host adaptation. RNA Biol. 2015;12(11):1169–77. https://doi.org/10.1080/15476286.2015.1094599 PMID: 26399159

72. Slonchak A, Parry R, Pullinger B, Sng JDJ, Wang X, Buck TF, et al. Structural analysis of 3'UTRs in insect flaviviruses reveals novel determinants of sfRNA biogenesis and provides new insights into flavivirus evolution. Nat Commun. 2022;13(1):1279. https://doi.org/10.1038/s41467-022-28977-3 PMID: 35277507

73. Gritsun TS, Gould EA. Origin and Evolution of 3'Utr of Flaviviruses: Long Direct Repeats as A Basis for the Formation of Secondary Structures and Their Significance for Virus Transmission. In: Advances in Virus Research [Internet]. Academic Press; 2006 [cited 2025 Apr 21]. p. 203–48. Available from: https://www.sciencedirect.com/science/article/pii/S0065352706690052

74. Gritsun TS, Gould EA. Direct repeats in the 3' untranslated regions of mosquito-borne flaviviruses: possible implications for virus transmission. J Gen Virol. 2006;87(11):3297–305.

75. Direct repeats in the flavivirus 3' untranslated region; a strategy for survival in the environment? Virology. 2007;358(2):258–65.

76. Zhang Q-Y, Li X-F, Niu X, Li N, Wang H-J, Deng C-L, et al. Short Direct Repeats in the 3' Untranslated Region Are Involved in Subgenomic Flaviviral RNA Production. J Virol. 2020;94(6):e01175-19. https://doi.org/10.1128/JVI.01175-19 PMID: 31896596

77. Zhang X, Li Y, Cao Y, Wu Y, Cheng G. The Role of Noncoding RNA in the Transmission and Pathogenicity of Flaviviruses. Viruses. 2024;16(2):242. https://doi.org/10.3390/v16020242 PMID: 38400018

78. Villordo SM, Gamarnik AV. Differential RNA sequence requirement for dengue virus replication in mosquito and mammalian cells. J Virol. 2013;87(16):9365–72. https://doi.org/10.1128/JVI.00567-13 PMID: 23760236

79. Mazeaud C, Freppel W, Chatel-Chaix L. The Multiples Fates of the Flavivirus RNA Genome During Pathogenesis. Front Genet. 2018;9:595. https://doi.org/10.3389/fgene.2018.00595 PMID: 30564270

80. Silva PAGC, Molenkamp R, Dalebout TJ, Charlier N, Neyts JH, Spaan WJM. Conservation of the pentanucleotide motif at the top of the yellow fever virus 17D 3' stem-loop structure is not required for replication. J Gen Virol. 2007;88(6):1738–47.

81. Elghonemy S, Davis WG, Brinton MA. The majority of the nucleotides in the top loop of the genomic 3' terminal stem loop structure are cis-acting in a West Nile virus infectious clone. Virology. 2005;331(2):238–46.

82. Tilgner M, Deas TS, Shi PY. The flavivirus-conserved penta-nucleotide in the 3' stem-loop of the West Nile virus genome requires a specific sequence and structure for RNA synthesis, but not for viral translation. Virology. 2005;331(2):375–86.

83. Plante JA, Plante KS, Popov VL, Shinde DP, Widen SG, Buenemann M, et al. Morphologic and Genetic Characterization of Ilheus Virus, a Potential Emergent Flavivirus in the Americas. Viruses. 2023;15(1):195. https://doi.org/10.3390/v15010195 PMID: 36680235

84. Jablunovsky A, Jose J. The Dynamic Landscape of Capsid Proteins and Viral RNA Interactions in Flavivirus Genome Packaging and Virus Assembly. Pathogens. 2024;13(2):120. https://doi.org/10.3390/pathogens13020120 PMID: 38392858

85. Mukhopadhyay S, Kuhn RJ, Rossmann MG. A structural perspective of the flavivirus life cycle. Nat Rev Microbiol. 2005;3(1):13–22. https://doi.org/10.1038/nrmicro1067 PMID: 15608696

86. Elshuber S, Mandl CW. Resuscitating mutations in a furin cleavage-deficient mutant of the flavivirus tick-borne encephalitis virus. J Virol. 2005;79(18):11813–23.

87. Zhang X, Jia R, Shen H, Wang M, Yin Z, Cheng A. Structures and Functions of the Envelope Glycoprotein in Flavivirus Infections. Viruses. 2017;9(11):338. https://doi.org/10.3390/v9110338 PMID: 29137162

88. Hu T, Wu Z, Wu S, Chen S, Cheng A. The key amino acids of E protein involved in early flavivirus infection: viral entry. Virol J. 2021;18(1):136. https://doi.org/10.1186/s12985-021-01611-2 PMID: 34217298

89. Roehrig JT, Volpe KE, Squires J, Hunt AR, Davis BS, Chang G-JJ. Contribution of disulfide bridging to epitope expression of the dengue type 2 virus envelope glycoprotein. J Virol. 2004;78(5):2648–52. https://doi.org/10.1128/jvi.78.5.2648-2652.2004 PMID: 14963174

90. Carbaugh DL, Lazear HM. Flavivirus envelope protein glycosylation: impacts on viral infection and pathogenesis. J Virol. 2020;94(11):e00104-20. https://doi.org/10.1128/JVI.00104-20

91. Ishida K, Yagi H, Kato Y, Morita E. N-linked glycosylation of flavivirus E protein contributes to viral particle formation. PLoS Pathog. 2023;19(10):e1011681. https://doi.org/10.1371/journal.ppat.1011681 PMID: 37819933

92. Zhang S, He Y, Wu Z, Wang M, Jia R, Zhu D, et al. Secretory pathways and multiple functions of nonstructural protein 1 in flavivirus infection. Front Immunol. 2023;14:1205002. https://doi.org/10.3389/fimmu.2023.1205002 PMID: 37520540

93. Rastogi M, Sharma N, Singh SK. Flavivirus NS1: a multifaceted enigmatic viral protein. Virol J. 2016;13:131. https://doi.org/10.1186/s12985-016-0590-7 PMID: 27473856

94. Akey DL, Brown WC, Dutta S, Konwerski J, Jose J, Jurkiw TJ, et al. Flavivirus NS1 crystal structures reveal a surface for membrane association and regions of interaction with the immune system. Science. 2014;343(6173):881–5.

95. Perera DR, Ranadeva ND, Sirisena K, Wijesinghe KJ. Roles of NS1 Protein in Flavivirus Pathogenesis. ACS Infect Dis. 2024;10(1):20–56. https://doi.org/10.1021/acsinfecdis.3c00566 PMID: 38110348

96. Huang S, Shi P-D, Fan X-X, Yang Y, Qin C-F, Zhao H, et al. The glycosylation deficiency of flavivirus NS1 attenuates virus replication through interfering with the formation of viral replication compartments. J Biomed Sci. 2024;31(1):60. https://doi.org/10.1186/s12929-024-01048-z PMID: 38849802

97. Fang E, Li M, Liu X, Hu K, Liu L, Zhang Z, et al. NS1 Protein N-Linked Glycosylation Site Affects the Virulence and Pathogenesis of Dengue Virus. Vaccines (Basel). 2023;11(5):959. https://doi.org/10.3390/vaccines11050959 PMID: 37243063

98. Dechtawewat T, Roytrakul S, Yingchutrakul Y, Charoenlappanit S, Siridechadilok B, Limjindaporn T. Potential phosphorylation of viral nonstructural protein 1 in dengue virus infection. Viruses. 2021;13(7):1393. https://doi.org/10.3390/v13071393

99. Zhang L, Wang H, Han C, Dong Q, Yan J, Guo W, et al. AMFR-mediated Flavivirus NS2A ubiquitination subverts ER-phagy to augment viral pathogenicity. Nat Commun. 2024;15(1):9578. https://doi.org/10.1038/s41467-024-54010-w PMID: 39505910

100. Yoon KJ, Song G, Qian X, Pan J, Xu D, Rho HS. Zika-virus-encoded NS2A disrupts mammalian cortical neurogenesis by degrading adherens junction proteins. Cell Stem Cell. 2017;21(3):349-358.e6. https://doi.org/10.1016/j.stem.2017.07.002

101. Wu R-H, Tsai M-H, Tsai K-N, Tian JN, Wu J-S, Wu S-Y, et al. Mutagenesis of Dengue Virus Protein NS2A Revealed a Novel Domain Responsible for Virus-Induced Cytopathic Effect and Interactions between NS2A and NS2B Transmembrane Segments. J Virol. 2017;91(12):e01836-16. https://doi.org/10.1128/JVI.01836-16 PMID: 28381578

102. Liu WJ, Wang XJ, Clark DC, Lobigs M, Hall RA, Khromykh AA. A single amino acid substitution in the West Nile virus nonstructural protein NS2A disables its ability to inhibit alpha/beta interferon induction and attenuates virus virulence in mice. J Virol. 2006;80(5):2396–404. https://doi.org/10.1128/JVI.80.5.2396-2404.2006 PMID: 16474146

103. Zhang X, Xie X, Xia H, Zou J, Huang L, Popov VL. Zika Virus NS2A-Mediated Virion Assembly. mBio. 2019;10(5):e02375-19. https://doi.org/10.1128/mBio.02375-19

104. Xie X, Zou J, Zhang X, Zhou Y, Routh AL, Kang C. Dengue NS2A Protein Orchestrates Virus Assembly. Cell Host Microbe. 2019;26(5):606-622.e8. https://doi.org/10.1016/j.chom.2019.09.007

105. Aguirre S, Luthra P, Sanchez-Aparicio MT, Maestre AM, Patel J, Lamothe F, et al. Dengue virus NS2B protein targets cGAS for degradation and prevents mitochondrial DNA sensing during infection. Nat Microbiol. 2017;2:17037. https://doi.org/10.1038/nmicrobiol.2017.37 PMID: 28346446

106. Kapoor M, Zhang L, Ramachandra M, Kusukawa J, Ebner KE, Padmanabhan R. Association between NS3 and NS5 proteins of dengue virus type 2 in the putative RNA replicase is linked to differential phosphorylation of NS5 *. J Biol Chem. 1995;270(32):19100–6.

107. Assenberg R, Mastrangelo E, Walter TS, Verma A, Milani M, Owens RJ. Crystal structure of a novel conformational state of the flavivirus NS3 protein: implications for polyprotein processing and viral replication. J Virol. 2009;83(24):12895–906.

108. Klaitong P, Smith DR. Roles of Non-Structural Protein 4A in Flavivirus Infection. Viruses. 2021;13(10):2077. https://doi.org/10.3390/v13102077 PMID: 34696510

109. Płaszczyca A, Scaturro P, Neufeldt CJ, Cortese M, Cerikan B, Ferla S, et al. A novel interaction between dengue virus nonstructural protein 1 and the NS4A-2K-4B precursor is required for viral RNA replication but not for formation of the membranous replication organelle. PLoS Pathog. 2019;15(5):e1007736. https://doi.org/10.1371/journal.ppat.1007736 PMID: 31071189

110. McLean JE, Wudzinska A, Datan E, Quaglino D, Zakeri Z. Flavivirus NS4A-induced autophagy protects cells against death and enhances virus replication. J Biol Chem. 2011;286(25):22147–59. https://doi.org/10.1074/jbc.M110.192500 PMID: 21511946

111. Morita E, Suzuki Y. Membrane-associated flavivirus replication complex—its organization and regulation. Viruses. 2021;13(6):1060.

112. Yau WL, Peters MBA, Sorin M, Rönfeldt S, Pulkkinen LIA, Carlson LA, et al. The flavivirus protein NS4B recruits the cis-Golgi protein ACBD3 to modify ER-Golgi trafficking for virion release [Internet]. bioRxiv; 2024 [cited 2025 May 2]. p. 2024.04.03.587877. Available from: https://www.biorxiv.org/content/10.1101/2024.04.03.587877v1

113. Goh JZH, De Hayr L, Khromykh AA, Slonchak A. The Flavivirus Non-Structural Protein 5 (NS5): Structure, Functions, and Targeting for Development of Vaccines and Therapeutics. Vaccines (Basel). 2024;12(8):865. https://doi.org/10.3390/vaccines12080865 PMID: 39203991

114. Bhattacharya D, Hoover S, Falk SP, Weisblum B, Vestling M, Striker R. Phosphorylation of Yellow Fever Virus NS5 Alters Methyltransferase Activity. Virology. 2008;380(2):276–84.

115. Brackney DE, Scott JC, Sagawa F, Woodward JE, Miller NA, Schilkey FD, et al. C6/36 Aedes albopictus cells have a dysfunctional antiviral RNA interference response. PLoS Negl Trop Dis. 2010;4(10):e856. https://doi.org/10.1371/journal.pntd.0000856 PMID: 21049065

116. Morazzani EM, Wiley MR, Murreddu MG, Adelman ZN, Myles KM. Production of virus-derived ping-pong-dependent piRNA-like small RNAs in the mosquito soma. PLoS Pathog. 2012;8(1):e1002470. https://doi.org/10.1371/journal.ppat.1002470 PMID: 22241995

117. Scott JC, Brackney DE, Campbell CL, Bondu-Hawkins V, Hjelle B, Ebel GD, et al. Comparison of dengue virus type 2-specific small RNAs from RNA interference-competent and -incompetent mosquito cells. PLoS Negl Trop Dis. 2010;4(10):e848. https://doi.org/10.1371/journal.pntd.0000848 PMID: 21049014

118. Göertz GP, Miesen P, Overheul GJ, van Rij RP, van Oers MM, Pijlman GP. Mosquito Small RNA Responses to West Nile and Insect-Specific Virus Infections in Aedes and Culex Mosquito Cells. Viruses. 2019;11(3):271. https://doi.org/10.3390/v11030271 PMID: 30889941

119. Altinli M, Leggewie M, Schulze J, Gyanwali R, Badusche M, Sreenu VB, et al. Antiviral RNAi Response in Culex quinquefasciatus-Derived HSU Cells. Viruses. 2023;15(2):436. https://doi.org/10.3390/v15020436 PMID: 36851650

120. Rückert C, Prasad AN, Garcia-Luna SM, Robison A, Grubaugh ND, Weger-Lucarelli J, et al. Small RNA responses of Culex mosquitoes and cell lines during acute and persistent virus infection. Insect Biochem Mol Biol. 2019;109:13–23. https://doi.org/10.1016/j.ibmb.2019.04.008 PMID: 30959110

121. Perdomo HD, Khorramnejad A, Cham NM, Kropf A, Sogliani D, Bonizzoni M. Prolonged exposure to heat enhances mosquito tolerance to viral infection. Commun Biol. 2025;8(1):1–10.

122. Oliveira JH, Bahia AC, Vale PF. How are arbovirus vectors able to tolerate infection? Dev Comp Immunol. 2020;103:103514. https://doi.org/10.1016/j.dci.2019.103514 PMID: 31585195

123. Goic B, Stapleford KA, Frangeul L, Doucet AJ, Gausson V, Blanc H, et al. Virus-derived DNA drives mosquito vector tolerance to arboviral infection. Nat Commun. 2016;7:12410. https://doi.org/10.1038/ncomms12410 PMID: 27580708

124. Hui L, Nie Y, Li S, Guo M, Yang W, Huang R, et al. Matrix metalloproteinase 9 facilitates Zika virus invasion of the testis by modulating the integrity of the blood-testis barrier. PLoS Pathog. 2020;16(4):e1008509. https://doi.org/10.1371/journal.ppat.1008509 PMID: 32302362

125. Leda AR, Bertrand L, Andras IE, El-Hage N, Nair M, Toborek M. Selective disruption of the blood–brain barrier by Zika virus. Frontiers in Microbiology. 2019;10:2158. https://doi.org/10.3389/fmicb.2019.02158

126. Moureau G, Cook S, Lemey P, Nougairede A, Forrester NL, Khasnatinov M, et al. New insights into flavivirus evolution, taxonomy and biogeographic history, extended by analysis of canonical and alternative coding sequences. PLoS One. 2015;10(2):e0117849. https://doi.org/10.1371/journal.pone.0117849 PMID: 25719412

127. Chong MK, Chua AJS, Tan TTT, Tan SH, Ng ML. Microscopy techniques in flavivirus research. Micron. 2014;59:33–43.

128. Schmidt HM, Horner SM. Towards a Universal Translator: Decoding the PTMs That Regulate Orthoflavivirus Infection. Viruses. 2025;17(2):287. https://doi.org/10.3390/v17020287 PMID: 40007042

129. Milhim BHGA, Estofolete CF, da Rocha LC, Liso E, Brienze VMS, Vasilakis N, et al. Fatal Outcome of Ilheus Virus in the Cerebrospinal Fluid of a Patient Diagnosed with Encephalitis. Viruses. 2020;12(9):957. https://doi.org/10.3390/v12090957 PMID: 32872425